AIAA JOURNAL
Vol. 42, No. 9, September 2004

Geometric and Kinematic Aspects of Image-Based Measurements of Deformable Bodies

Tianshu Liu*
NASA Langley Research Center, Hampton, Virginia 23681-0001

From the viewpoint of an experimental fluid dynamicist, theoretical foundations of quantitative image-based measurements for extracting geometric and kinematic properties of deformable bodies like fluids are discussed. New results are obtained by using a combination of methods in perspective and differential geometry and continuum mechanics. Topics include perspective projection transformation, perspective developable conical surface and its applications, perspective projection of motion field on surface, the correspondence problem, composite image space, perspective invariants, and motion equations of image intensity. The developed methods provide useful tools for experimentalists to determine morphology and motion field of deformable bodies from images.

Nomenclature

$\boldsymbol{A}$	=	matrix defined in Eq. (5) related to the interior orientation parameters
$\boldsymbol{B}$	=	binormal vector of a curve in the object space
c	=	principal distance
D_{ij}	=	distance from a point $\boldsymbol{X}_i$ to the osculating plane to a curve at the point $\boldsymbol{X}_j$
I	=	image intensity
L	=	radiance
$\boldsymbol{M}$	=	$[m_{ij}]$, rotational matrix
$\boldsymbol{M}_h$	=	$(\boldsymbol{M} - \boldsymbol{M}\boldsymbol{X}_c)$, extended rotational matrix (3×4)
$\boldsymbol{m}_1, \boldsymbol{m}_2, \boldsymbol{m}_3$	=	row vectors in the rotational matrix $\boldsymbol{M} = [m_{ij}]$
$\boldsymbol{N}$	=	normal vector on a curve or a surface in the object space
$\boldsymbol{P}$	=	$\boldsymbol{A}^{-1}\boldsymbol{M}$, matrix describing the relationship between $\boldsymbol{x}_h$ and $\boldsymbol{X} - \boldsymbol{X}_c$
$\bar{P}$	=	$M^{-1}A$, inverse matrix of P
$\boldsymbol{P}_h$	=	$\boldsymbol{A}^{-1}\boldsymbol{M}_h$, extended matrix of $\boldsymbol{P}$ (3×4)
$\bar{\boldsymbol{P}}_{32}$	=	matrix composed of the first two columns of $\bar{\boldsymbol{P}}$
$\boldsymbol{T}$	=	tangential vector of a curve
$\boldsymbol{U}(\boldsymbol{X})$	=	$\mathrm{d}\boldsymbol{X}/\mathrm{d}t$, motion field in the object space
$\boldsymbol{U}_{12}$	=	$(U_1, U_2)^T$, two-dimensional velocity vector of $\boldsymbol{U}(\boldsymbol{X})$
$\langle \boldsymbol{U}_{12} \rangle_\psi$	=	average two-dimensional velocity vector in terms of the scalar density ψ
$\langle \boldsymbol{U}_{12} \rangle_\rho$	=	average two-dimensional velocity vector in terms of the fluid density ρ
$\boldsymbol{u}$	=	$\mathrm{d}\boldsymbol{x}/\mathrm{d}t$, optical flow in the image plane
$\boldsymbol{W}_1, \boldsymbol{W}_2$	=	vectors composed of $\boldsymbol{m}_1, \boldsymbol{m}_2, \boldsymbol{m}_3$
$\boldsymbol{X}$	=	$(X^1, X^2, X^3)^T$, object space coordinates
$\boldsymbol{X}_c$	=	$(X_c^1, X_c^2, X_c^3)^T$, location of the perspective center (optical center)
$\boldsymbol{X}_h$	=	$(X^1, X^2, X^3, 1)^T$, homogeneous object space coordinates
$\bar{\boldsymbol{X}}$	=	$\boldsymbol{M}(\boldsymbol{X} - \boldsymbol{X}_c)$, projection of $\boldsymbol{X} - \boldsymbol{X}_c$ on $\boldsymbol{m}_1, \boldsymbol{m}_2, \boldsymbol{m}_3$
$\boldsymbol{x}$	=	$(x^1, x^2)^T$, image coordinates
$\boldsymbol{x}_{\mathrm{com}}$	=	$(x_{(1)}^1, x_{(1)}^2, x_{(2)}^1)^T$, composite image coordinates
$\boldsymbol{x}_h$	=	$(x^1, x^2, 1)^T$, homogeneous image coordinates
$\boldsymbol{x}_p$	=	$(x_p^1, x_p^2)^T$, principal-point location in the image plane
κ_c, κ_{C_p}	=	curvature of curve C or C_P
$\kappa_{\mathrm{obj}}, \kappa_{\mathrm{im}}$	=	curvature of curve in the object space and composite image space
λ	=	$-c/\boldsymbol{m}_3 \cdot (\boldsymbol{X} - \boldsymbol{X}_c)$, scaling factor
ρ	=	fluid density
$\tau_{\mathrm{obj}}, \tau_{\mathrm{im}}$	=	torsion of curve in the object space and composite image space
ω, ϕ, κ	=	Euler orientation angles of camera

Received 16 April 2003; accepted for publication 3 May 2004.

*Research Scientist, MS 238; t.liu@larc.nasa.gov. Member AIAA.

I. Introduction

IMAGE-BASED measurement techniques play an increasingly important role in virtually all natural sciences and engineering disciplines because they can provide tremendous information and knowledge about observed objects in a global, noncontact way with high temporal and spatial resolution. Specialists in photogrammetry, computer vision, and other scientific disciplines have developed various methods that are best suitable to particular applications in their fields. In particular, both photogrammetrists and computer-vision scientists have studied image-based techniques to obtain geometric information. The approaches developed by photogrammetrists are more mature and quantitative, which are recently extended to nontopographic applications.[1] By contrast, in order to deal with more complicated vision problems related to artificial intelligence, computer-vision scientists have adopted more versatile mathematical methods in perspective geometry, differential geometry, and image algebra.[2–5] However, the approaches used by computer-vision scientists are of qualitative nature in many cases and generally less accurate than those used in photogrammetry in metric measurements. Because the objectives of various disciplines are different, there is a lack of sufficient interaction among specialists in these technical communities. Perhaps because of different notations, jargons, and methodologies in these communities, it is difficult to transcend the different technical domains and see a unified scope of various image techniques. On the other hand, most of experimental fluid dynamicists are not aware of various image-based techniques developed in photogrammetry and computer vision, which can be useful for measurements of motion fields and physical quantities of fluid flows. Unlike photogrammetrists and computer-vision scientists who mainly study rigid bodies, experimental fluid dynamicists have to deal with complex morphology and motion field of deformable bodies like fluids. Therefore, it is highly desirable to integrate various techniques into a unified theoretical framework for experimental fluid dynamicists.

This paper discusses the geometric and kinematic aspects of quantitative image-based measurements of morphology and motion field of deformable bodies. Emphasis is placed on the general principles and methodologies rather than detailed solution techniques and

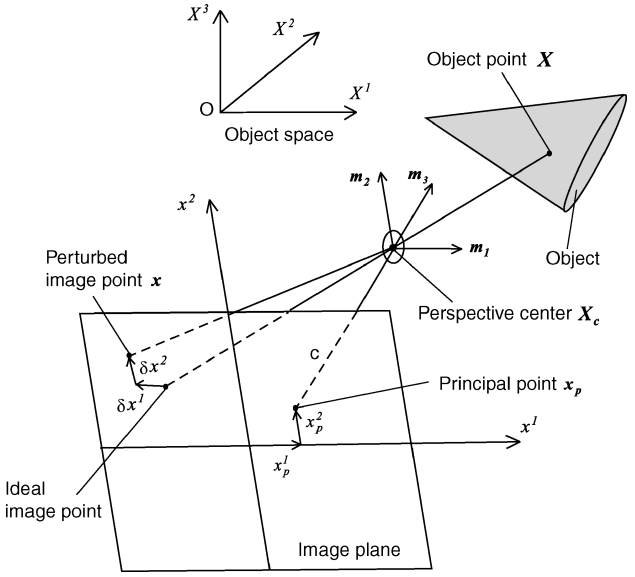

Fig. 1 Imaging geometry and coordinate systems.

algorithms. First, we provide a unified treatment of the perspective projection transformation from the three-dimensional object space (three-dimensional physical space) to the two-dimensional image and illustrate geometric connection between different formulations of the perspective projection transformation. Next, we discuss some fundamental problems for recovering geometry and motion of deformable bodies. They are projective developable conical surface and its applications, reconstruction of motion field of space curve and motion field constrained on surface, the correspondence problem, composite image space, and projective invariants. These problems are related to a number of techniques in experimental fluid mechanics, including particle-tracking velocimetry, stereoscopic particle-image velocimetry, laser-tagging fluorescence technique, and other flow-visualization techniques. Motion equations of the image intensity are derived for typical transport processes of passive scalar and density-varying flows. These equations can be used to reconstruct the motion fields of fluid flows from fluorescence images, transmittance images, schlieren images, and shadowgraph images of moving patterns.

II. Perspective Projection Transformation

There is a perspective projection transformation between the three-dimensional object space coordinates $\boldsymbol{X}=(X^1, X^2, X^3)^T$ and the corresponding two-dimensional image coordinates $\boldsymbol{x}=(x^1, x^2)^T$ (Refs. 1 and 6–8). Figure 1 illustrates the camera imaging process. The image and object space coordinates are related by the following collinearity condition:

$$\begin{pmatrix} x^1 - x_p^1 + \delta x^1 \\ x^2 - x_p^2 + \delta x^2 \\ -c \end{pmatrix} = \lambda \boldsymbol{M} \begin{pmatrix} X^1 - X_c^1 \\ X^2 - X_c^2 \\ X^3 - X_c^3 \end{pmatrix} \tag{1}$$

where $\boldsymbol{X}_c=(X_c^1, X_c^2, X_c^3)^T$ is the perspective center or optical center and the shifts δx^1 and δx^2 represent the lens distortion. The elements of the rotation matrix $\boldsymbol{M}=[m_{ij}](i, j=1, 2, 3)$ are functions of the Euler orientation angles (ω, ϕ, κ):

$$m_{11}=\cos\phi\cos\kappa, \qquad m_{12}=\sin\omega\sin\phi\cos\kappa+\cos\omega\sin\kappa$$

$$m_{13}=-\cos\omega\sin\phi\cos\kappa+\sin\omega\sin\kappa, \qquad m_{21}=-\cos\phi\sin\kappa$$

$$m_{22}=-\sin\omega\sin\phi\sin\kappa+\cos\omega\cos\kappa$$

$$m_{23}=\cos\omega\sin\phi\sin\kappa+\sin\omega\cos\kappa, \qquad m_{31}=\sin\phi$$

$$m_{32}=-\sin\omega\cos\phi, \qquad m_{33}=\cos\omega\cos\phi \tag{2}$$

Loosely speaking, the orientation angles (ω, ϕ, κ) are the pitch, yaw, and roll angles of the camera in the established coordinate system in the object space. The rotational matrix $\boldsymbol{M}$ is an orthogonal matrix having the property of $\boldsymbol{M}^{-1}=\boldsymbol{M}^T$.

Algebraic manipulation of Eq. (1) yields the well-known collinearity equations relating the object space point to the corresponding image point:

$$x^1 - x_p^1 + \delta x^1 = -c\frac{\boldsymbol{m}_1\cdot(\boldsymbol{X}-\boldsymbol{X}_c)}{\boldsymbol{m}_3\cdot(\boldsymbol{X}-\boldsymbol{X}_c)} = -c\frac{\bar{X}^1}{\bar{X}^3}$$

$$x^2 - x_p^2 + \delta x^2 = -c\frac{\boldsymbol{m}_2\cdot(\boldsymbol{X}-\boldsymbol{X}_c)}{\boldsymbol{m}_3\cdot(\boldsymbol{X}-\boldsymbol{X}_c)} = -c\frac{\bar{X}^2}{\bar{X}^3} \tag{3}$$

The vectors $\boldsymbol{m}_1=(m_{11}, m_{12}, m_{13})^T$ and $\boldsymbol{m}_2=(m_{21}, m_{22}, m_{23})^T$ are the directional cosine vectors parallel to the x^1 axis and x^2 axis in the image plane, respectively. The vector $\boldsymbol{m}_3=(m_{31}, m_{32}, m_{33})^T$ is normal to the image plane, directing from the principal point to the optical center along the optical axis. As shown in Fig. 1, the unit orthogonal vectors $\boldsymbol{m}_1$, $\boldsymbol{m}_2$, and $\boldsymbol{m}_3$ $(\boldsymbol{m}_i\cdot\boldsymbol{m}_j=\delta_{ij})$ constitute a local object space coordinate frame at the optical center $\boldsymbol{X}_c$. The coordinates $\bar{\boldsymbol{X}}=(\bar{X}^1, \bar{X}^2, \bar{X}^3)^T$ are the projections of the object space position vector $\boldsymbol{X}-\boldsymbol{X}_c$ in this frame. The scaling factor $\lambda=-c/\boldsymbol{m}_3\cdot(\boldsymbol{X}-\boldsymbol{X}_c)$ is a ratio between the principal distance and the projected component of the object space position vector $\boldsymbol{X}-\boldsymbol{X}_c$ on the optical axis along $-\boldsymbol{m}_3$ direction. When a point $\boldsymbol{X}$ is on the focal plane $\boldsymbol{m}_3\cdot(\boldsymbol{X}-\boldsymbol{X}_c)=0$, the scaling factor becomes infinite $(\lambda=\infty)$, which corresponds to the points at infinity on the image plane. The terms δx^1 and δx^2 in Eq. (3) are the image coordinate shifts produced by lens distortion, which are modeled by a sum of the radial and decentering distortion terms.[6,9] They are characterized by the radial distortion parameters K_1 and K_2 and the decentering distortion parameters P_1 and P_2 in a polynomial model of lens distortion.[6,9]

Equation (3) can be rewritten in the homogeneous image coordinates $\boldsymbol{x}_h=(x^1, x^2, 1)^T$

$$\boldsymbol{x}_h=\lambda\boldsymbol{P}(\boldsymbol{X}-\boldsymbol{X}_c) \tag{4}$$

where the matrix $\boldsymbol{P}=[p_{ij}]=\boldsymbol{A}^{-1}\boldsymbol{M}$ describes the relationship between $\boldsymbol{x}_h$ and $\boldsymbol{X}-\boldsymbol{X}_c$ and $\boldsymbol{A}=[a_{ij}]$, defined as

$$\boldsymbol{A}=\begin{pmatrix} 1 & 0 & -x_p^1+\delta x^1 \\ 0 & 1 & -x_p^2+\delta x^2 \\ 0 & 0 & -c \end{pmatrix} \tag{5}$$

is related to the interior orientation parameters. A tensor form of Eq. (4) is $a_{ij}x_k^j=\lambda m_{ij}(X^j-X_c^j)$. Here, the Einstein convention for summation is used throughout the paper. The tensor form of the collinearity equations is convenient for mathematical manipulation. Another alternative form of the collinearity equations in the homogeneous coordinates is

$$\boldsymbol{x}_h=\lambda\boldsymbol{P}_h\boldsymbol{X}_h \tag{6}$$

Although Eqs. (4) and (6) are formally written as a linear relation between $\boldsymbol{x}_h$ and $\boldsymbol{X}$ or $\boldsymbol{X}_h$, they are essentially nonlinear because not only are the lens distortion terms a nonlinear function of $\boldsymbol{x}$ but also the scaling factor $\lambda=-c/\boldsymbol{m}_3\cdot(\boldsymbol{X}-\boldsymbol{X}_c)$ is not a constant in general.

Furthermore, Eq. (3) can be rewritten as a form suitable to least-squares estimation for the object space coordinates $\boldsymbol{X}$:

$$\boldsymbol{W}_1\cdot(\boldsymbol{X}-\boldsymbol{X}_c)=0, \qquad \boldsymbol{W}_2\cdot(\boldsymbol{X}-\boldsymbol{X}_c)=0 \tag{7}$$

where $\boldsymbol{W}_1$ and $\boldsymbol{W}_2$ are defined as $\boldsymbol{W}_1=(x^1-x_p^1+\delta x^1)\boldsymbol{m}_3+c\boldsymbol{m}_1$ and $\boldsymbol{W}_2=(x^2-x_p^2+\delta x^2)\boldsymbol{m}_3+c\boldsymbol{m}_2$. As shown in Fig. 2, the vector $\boldsymbol{W}_1$ is on the plane spanned by the orthogonal unit vectors $\boldsymbol{m}_1$ and $\boldsymbol{m}_3$, while $\boldsymbol{W}_2$ is on a plane spanned by $\boldsymbol{m}_2$ and $\boldsymbol{m}_3$. Geometrically, Eq. (7) describes two planes normal to $\boldsymbol{W}_1$ and $\boldsymbol{W}_2$, defining an intersection line of the two planes through the optical center $\boldsymbol{X}_c$. For a given image point $\boldsymbol{x}=(x^1, x^2)^T$, Eq. (7) is not sufficient to determine the object space point with the three unknown coordinates

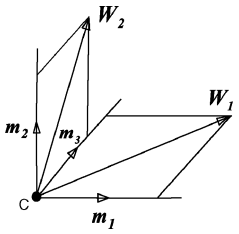

Fig. 2 Relation between the vectors m_i and W_i ($i = 1, 2, 3$).

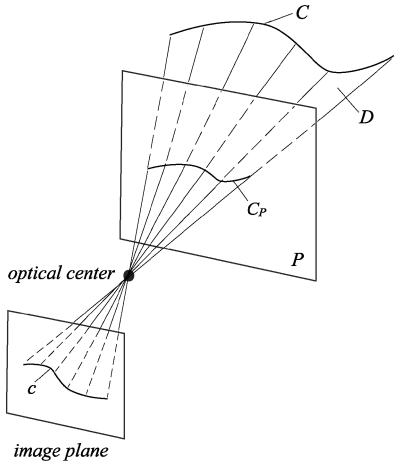

Fig. 3 Perspective developable conical surface containing a three-dimensional space curve.

$\boldsymbol{X} = (X^1, X^2, X^3)^T$. Hence, extra equations associated with additional cameras and other geometrical constraints should be added to find a unique least-squares solution of $\boldsymbol{X}$. The collinearity equations contain the exterior orientation parameters $(\omega, \phi, \kappa, X_c^1, X_c^2, X_c^3)$, interior orientation parameters (c, x_p^1, x_p^2), and lens distortion parameters (K_1, K_2, P_1, P_2). Geometric calibration of camera for determining these parameters is an important and active topic in quantitative image-based measurements.[10–14] Throughout this paper, we generally assume that cameras are calibrated such that these parameters are known.

III. Projective Developable Conical Surface and Its Applications

A. Generating Projective Developable Conical Surface

The concept of the projective developable conical surface is introduced. In principle, a three-dimensional curve in the object space cannot be completely recovered from a single image because information in one dimension is lost in projection. Nevertheless, using a calibrated camera, the projective conical developable surface on which a three-dimensional curve lies can be reconstructed. Further, when two calibrated cameras are used, a three-dimensional curve can be uniquely determined as an intersection of two projective conical developable surfaces.

Consider a curve C in the object space. As shown Fig. 3, it is projected onto the image plane and a plane P normal to the optical axis (parallel to the image plane). Equation (4) is written as

$$\boldsymbol{X} - \boldsymbol{X}_c = \lambda^{-1}\bar{\boldsymbol{P}}\boldsymbol{x}_h \tag{8}$$

where $\bar{\boldsymbol{P}} = \boldsymbol{P}^{-1} = [\bar{p}_{ij}] = \boldsymbol{M}^{-1}\boldsymbol{A} = \boldsymbol{M}^T\boldsymbol{A}$ is the inverse matrix of $\boldsymbol{P}$. For the given camera orientation parameters, assuming that the lens distortion parameters are fixed and the scaling factor λ is constant, we have a differential relation

$$\mathrm{d}\boldsymbol{X} = \lambda^{-1}\bar{\boldsymbol{P}}_{32}\,\mathrm{d}\boldsymbol{x} \tag{9}$$

where $\mathrm{d}\boldsymbol{X} = (\mathrm{d}X^1, \mathrm{d}X^2, \mathrm{d}X^3)^T$, $\mathrm{d}\boldsymbol{x} = (\mathrm{d}x^1, \mathrm{d}x^2)^T$, and $\bar{\boldsymbol{P}}_{32} = [\bar{p}_{ij}]$ is a 3×2 matrix ($i = 1, 2, 3$; $i = 1, 2$) composed of the first two columns of $\bar{\boldsymbol{P}}$. A constraint imposed on Eq. (9) is $\mathrm{d}\lambda = 0$ or $\boldsymbol{m}_3 \cdot \mathrm{d}\boldsymbol{X} = 0$, indicating that Eq. (9) actually describes the projection C_P of the curve C on the plane P orthogonal to the optical axis direction or $\boldsymbol{m}_3$. In fact, as shown in Fig. 3, $\lambda = -c/\boldsymbol{m}_3 \cdot (\boldsymbol{X} - \boldsymbol{X}_c) = \text{const}$ defines the plane P. For $\lambda < 0$, the plane P is in the half-space that the vector $\boldsymbol{m}_3$ points to from the optical center, while for $\lambda > 0$ the plane P is in another half of space along with the image plane. As $|\lambda| \to \infty$, the plane P approaches to the optical center, and the plane goes to infinity as $|\lambda| \to 0$. As shown in Fig. 3, the projected curve C_P on the plane P can be reconstructed from image measurement, and the developable conical surface D containing the three-dimensional curve C can be generated consequently.

The arc length element of the projected curve C_P on the plane P is $\mathrm{d}S_{C_P} = |\mathrm{d}\boldsymbol{X}| = \lambda^{-1}|\bar{\boldsymbol{P}}_{32}\boldsymbol{t}|\mathrm{d}s$, where $\boldsymbol{t} = \mathrm{d}\boldsymbol{x}/\mathrm{d}s$ and $\mathrm{d}s = |\mathrm{d}\boldsymbol{x}|$ are the unit tangent vector and arc length element of the projected curve on the image plane, respectively. Clearly, when the plane P moves to infinity as $|\lambda| \to 0$, the arc length of the curve C_P becomes infinitely large. Furthermore, the curvature κ_{C_P} of C_P and the corresponding curvature κ_c in the image plane can be calculated. The ratio κ_{C_P}/κ_c is proportional to the scaling factor λ. When the plane P moves to infinity as $|\lambda| \to 0$, the curvature of the curve C_P becomes smaller and smaller because the curve is spreading.

The unit tangent vector of the projected curve C_P on the plane P is related to the image coordinates by $\boldsymbol{T}_{C_P} = \mathrm{d}\boldsymbol{X}/\mathrm{d}S_{C_P} = \bar{\boldsymbol{P}}_{32}\boldsymbol{t}/|\bar{\boldsymbol{P}}_{32}\boldsymbol{t}|$. The projected curve C_P on the plane P is given by

$$\boldsymbol{X}_{C_P} = \boldsymbol{X}_{C_P0} + \int_0^{S_{C_P}} \boldsymbol{T}_{C_P}\left(S_{C_P}\right)\mathrm{d}S_{C_P} \tag{10}$$

The initial position $\boldsymbol{X}_{C_P0} = \boldsymbol{X}_c + \lambda^{-1}\bar{\boldsymbol{P}}\boldsymbol{x}_{h0}$ on the projected curve C_P in the object space is conveniently chosen at the endpoint of the curve, where $\boldsymbol{x}_{h0} = (x_0^1, x_0^2, 1)^T$ is the homogeneous coordinates of the corresponding image point to $\boldsymbol{X}_{C_P0}$. Substitution of the expressions for $\mathrm{d}S_{C_P}$, $\boldsymbol{X}_{C_P0}$, and $\boldsymbol{T}_{C_P}$ into Eq. (10) leads to a projective ray vector directing from the optical center $\boldsymbol{X}_c$ to a point $\boldsymbol{X}_{C_P}$ on the projected curve C_P:

$$\boldsymbol{X}_{C_P} - \boldsymbol{X}_c = \lambda^{-1}\left(\bar{\boldsymbol{P}}\boldsymbol{x}_{h0} + \int_0^s \bar{\boldsymbol{P}}_{32}\boldsymbol{t}\,\mathrm{d}s\right) \tag{11}$$

A family of the projective rays through the optical center $\boldsymbol{X}_c$ given by Eq. (11) generates a projective developable conical surface D that contains the three-dimensional curve C. A single-parameter family of the tangent planes on the developable conical surface D is given by $(\boldsymbol{X} - \boldsymbol{X}_c) \cdot \boldsymbol{N}_D(s) = 0$, where the arc length s of the projected curve in the image plane is an adjustable parameter and $\boldsymbol{N}_D(s) = \boldsymbol{T}_{C_P} \times (\boldsymbol{X}_{C_P} - \boldsymbol{X}_c)/|\boldsymbol{T}_{C_P} \times (\boldsymbol{X}_{C_P} - \boldsymbol{X}_c)|$ is the unit normal vector to the tangent plane on the developable surface. The projective conical developable surface is an envelope generated by a family of the tangent planes, which is given by $(\boldsymbol{X} - \boldsymbol{X}_c) \cdot \boldsymbol{N}_D(s) = 0$ and $(\boldsymbol{X} - \boldsymbol{X}_c) \cdot \mathrm{d}\boldsymbol{N}_D(s)/\mathrm{d}s = 0$ (Ref. 15). Thus, the projective developable conical surface is reconstructed from measured image quantities.

B. Reconstructing Three-Dimensional Curve and Its Motion

From a single image, we reconstruct the projective conical developable surface containing a three-dimensional curve C rather than the curve itself. Nevertheless, when two calibrated cameras are used, as shown in Fig. 4, the curve C can be uniquely determined by intersecting the two projective developable conical surfaces associated with the different cameras. Use of more cameras could increase the redundancy of calculation and improve the accuracy. In experimental fluid mechanics, marked tracer lines such as hydrogen bubble lines and laser-tagging fluorescence lines are used for flow visualization. The projective developable conical surfaces allow quantitative recovery of geometry and motion of these tracer lines evolved in complex flows. Note that a three-dimensional solid surface in the object space can be reconstructed from a family of the developable conical surfaces containing the contours of the surface.

After a moving three-dimensional curve in the object space is reconstructed from images at successive instants, we can determine the motion field $\boldsymbol{U}(\boldsymbol{X}) = \mathrm{d}\boldsymbol{X}/\mathrm{d}t$ of the curve. The curve is given by

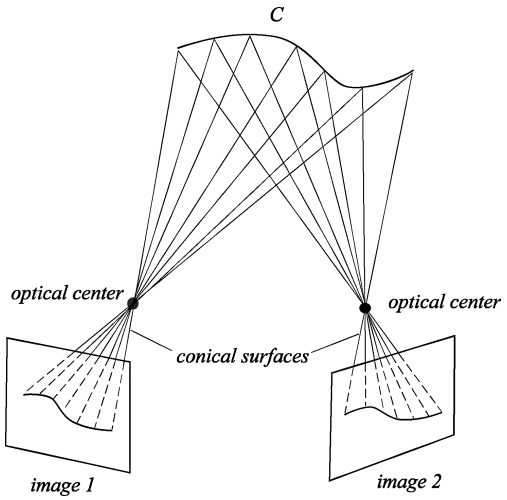

Fig. 4 Intersection between two developable conical surfaces.

$\boldsymbol{X} = \boldsymbol{X}[S(t), t]$, where t is time and $S(t)$ is the arc length of the curve in the object space. In general, the temporal and spatial difference $\Delta_{St}\boldsymbol{X} = \boldsymbol{X}[S(t_2), t_2] - \boldsymbol{X}[S(t_1), t_1]$ at two successive instants t_1 and t_2 (the time interval $\Delta t = t_2 - t_1$ is small) is obtained from measurements. Reconstruction of the motion field of the curve from $\Delta_{St}\boldsymbol{X}$ is nontrivial because the point correspondence between two sequential images is not known without using distinct targets (marks) on a deforming curve. To increase the determinability of the problem, the motion field of the curve should be constrained by underlying physical mechanisms behind the motion and deformation of the curve. In general, reconstruction of the motion field is formulated as an optimization problem $\|\Delta_{St}\boldsymbol{X} - \boldsymbol{U}(\boldsymbol{X})\Delta t\| \rightarrow \min$ subject to relevant physical and geometric constraints.

In the simplest case in which the curve is rigid, the rigid-body motion of the curve is described by $\boldsymbol{U}(\boldsymbol{X}) = \boldsymbol{U}_0 + \Omega_0 \times (\boldsymbol{X} - \boldsymbol{X}_0)$, where $\boldsymbol{U}_0$ and Ω_0 are the constant translation velocity and angular velocity, respectively, and $\boldsymbol{X}_0$ is the rotational center of the curve. There are six unknowns in $\boldsymbol{U}_0$ and Ω_0 for optimization. A slightly more complicated case is that the curve is stretched in three fixed directions in addition to the rigid-body motion. Thus, addition of the three stretching constants leads to nine unknowns for optimization. Furthermore, for a highly deforming material line in the incompressible and irrotational flow, the physical constraints are the solenoidal and irrotational conditions $\nabla \cdot \boldsymbol{U}(\boldsymbol{X}) = 0$ and $\nabla \times \boldsymbol{U}(\boldsymbol{X}) = 0$ (Ref. 16). A vortex filament in the incompressible and irrotational flow is an interesting case where the filament is no longer passive and the self-induced motion field is directly proportional to the curvature of the filament along the binormal direction vector.[17]

C. Determining Three-Dimensional Displacement Vector

Using the perspective developable conical surfaces, we can determine the displacement vector in the object space from the corresponding projected displacement vectors on the image planes. This problem is related to stereoscopic particle image velocimetry.[18,19] In stereoscopic particle image velocimetry, the displacement vectors of a moving particle group in the image plane between two successive instants are first obtained using the pattern correlation techniques. Then the displacement vector averaged over the particle group in the object space is recovered using stereoscopy because the point correspondence between the two images on a constrained surface (e.g., a thin laser sheet) is one to one (see Sec. IV). Previous stereoscopic analysis given by Arroyo and Greated[18] and Prasad and Adrian[19] was two dimensional under particular geometric conditions in which the image planes are in parallel to the illuminating laser sheet. Here, a general analysis is provided for recovering the displacement vector by utilizing the perspective developable conical surfaces.

Figure 5 shows the displacement vector $\boldsymbol{X}_1 - \boldsymbol{X}_0$ in the object space and the corresponding projected displacement vectors $\boldsymbol{x}_{1(1)} - \boldsymbol{x}_{0(1)}$ on image 1 and $\boldsymbol{x}_{1(2)} - \boldsymbol{x}_{0(2)}$ on image 2. Images 1 and 2 are taken by two cameras whose the perspective centers are located at

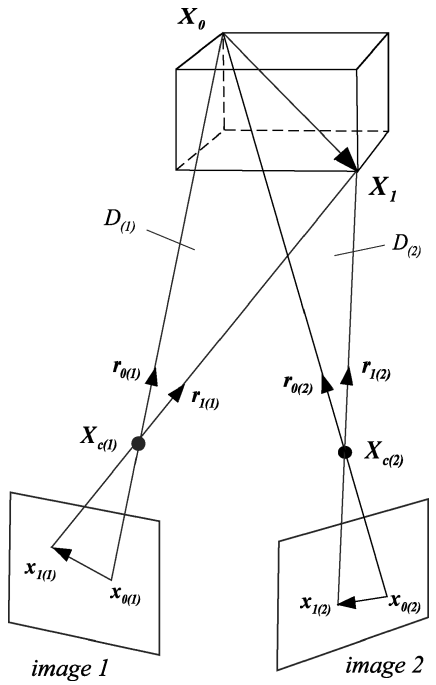

Fig. 5 Displacement vector in the object space and its projected vectors in images 1 and 2.

$\boldsymbol{X}_{c(1)}$ and $\boldsymbol{X}_{c(2)}$, respectively. The subscript $(i) = 1, 2$ denotes cameras 1 and 2. Because the projected displacement vectors on the images are the straight lines with the constant tangential vectors, Eq. (11) can be simplified for the projective rays from the endpoints of the displacement vectors in the image plane to the corresponding endpoints of the displacement vector in the object space. The ray vectors from the image points $\boldsymbol{x}_{1(1)}, \boldsymbol{x}_{0(1)}, \boldsymbol{x}_{1(2)}$, and $\boldsymbol{x}_{0(2)}$ to the object space points $\boldsymbol{X}_1$ and $\boldsymbol{X}_0$ are described by

$$\begin{aligned}
\boldsymbol{X}_0 - \boldsymbol{X}_{c(1)} &= \lambda_{0(1)}^{-1} \bar{\boldsymbol{P}}_{(1)} \boldsymbol{x}_{h0(1)} \\
\boldsymbol{X}_1 - \boldsymbol{X}_{c(1)} &= \lambda_{1(1)}^{-1} \left(\bar{\boldsymbol{P}}_{(1)} \boldsymbol{x}_{h0(1)} + \bar{\boldsymbol{P}}_{32(1)} \boldsymbol{t}_{(1)} s_{(1)} \right) \\
\boldsymbol{X}_0 - \boldsymbol{X}_{c(2)} &= \lambda_{0(2)}^{-1} \bar{\boldsymbol{P}}_{(2)} \boldsymbol{x}_{h0(2)} \\
\boldsymbol{X}_1 - \boldsymbol{X}_{c(2)} &= \lambda_{1(2)}^{-1} \left(\bar{\boldsymbol{P}}_{(2)} \boldsymbol{x}_{h0(2)} + \bar{\boldsymbol{P}}_{32(2)} \boldsymbol{t}_{(2)} s_{(2)} \right)
\end{aligned} \tag{12}$$

The projected displacement vectors on images 1 and 2 are $\boldsymbol{x}_{1(i)} - \boldsymbol{x}_{0(i)} = \boldsymbol{t}_{(i)} s_{(i)} (i = 1, 2)$, where the unit tangential vectors $\boldsymbol{t}_{(i)}$ and the lengths $s_{(i)}$ of the projected displacement vectors are measured in the image plane. For calibrated cameras, the matrices $\bar{\boldsymbol{P}}_{(i)}$ and $\bar{\boldsymbol{P}}_{32(i)}$ in Eq. (12) are known. In general, the scaling factors $\lambda_{0(i)}$ and $\lambda_{1(i)}$ are not constants except in a special case where a particle moves on the plane (e.g., the laser sheet) parallel to the image planes. Nevertheless, the unit ray vectors are not dependent of the scaling factors, which are given by

$$\begin{aligned}
\boldsymbol{r}_{0(1)} &= \left(\boldsymbol{X}_0 - \boldsymbol{X}_{c(1)} \right) \Big/ \left| \boldsymbol{X}_0 - \boldsymbol{X}_{c(1)} \right| \\
\boldsymbol{r}_{1(1)} &= \left(\boldsymbol{X}_1 - \boldsymbol{X}_{c(1)} \right) \Big/ \left| \boldsymbol{X}_1 - \boldsymbol{X}_{c(1)} \right| \\
\boldsymbol{r}_{0(2)} &= \left(\boldsymbol{X}_0 - \boldsymbol{X}_{c(2)} \right) \Big/ \left| \boldsymbol{X}_0 - \boldsymbol{X}_{c(2)} \right| \\
\boldsymbol{r}_{1(2)} &= \left(\boldsymbol{X}_1 - \boldsymbol{X}_{c(2)} \right) \Big/ \left| \boldsymbol{X}_1 - \boldsymbol{X}_{c(2)} \right|
\end{aligned} \tag{13}$$

The unit ray vectors can be determined using the image coordinates through Eq. (12). As shown in Fig. 6, the unit ray vectors $\boldsymbol{r}_{0(1)}$ and $\boldsymbol{r}_{1(1)}$ give a projective developable conical plane $D_{(1)}$, i.e., $(\boldsymbol{X} - \boldsymbol{X}_{c(1)}) \cdot (\boldsymbol{r}_{1(1)} \times \boldsymbol{r}_{0(1)}) = 0$. In the same way, the unit ray vectors $\boldsymbol{r}_{0(2)}$ and $\boldsymbol{r}_{1(2)}$ constitute another projective developable conical plane $D_{(2)}$, i.e., $(\boldsymbol{X} - \boldsymbol{X}_{c(2)}) \cdot (\boldsymbol{r}_{1(2)} \times \boldsymbol{r}_{0(2)}) = 0$. Clearly, the displacement vector $\boldsymbol{X}_1 - \boldsymbol{X}_0$ in the object space is on the intersection line between the projective developable conical planes $D_{(1)}$ and

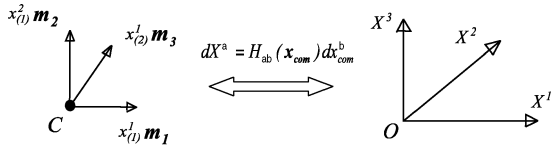

Fig. 6 Composite image space and object space.

$D_{(2)}$. The angle between the two planes $D_{(1)}$ and $D_{(2)}$ is given by $\cos\alpha = (\boldsymbol{r}_{1(1)} \times \boldsymbol{r}_{0(1)}) \cdot (\boldsymbol{r}_{1(2)} \times \boldsymbol{r}_{0(2)})/|\boldsymbol{r}_{1(1)} \times \boldsymbol{r}_{0(1)}||\boldsymbol{r}_{1(2)} \times \boldsymbol{r}_{0(2)}|$. When the absolute value of the angle $|\alpha|(\leq \pi/2)$ is large, the determination of the displacement vector $\boldsymbol{X}_1 - \boldsymbol{X}_0$ in the object space is less sensitive to errors in image measurements. For a singular case where $|\alpha| = 0$, the displacement vector $\boldsymbol{X}_1 - \boldsymbol{X}_0$ cannot be recovered.

Ideally, the endpoint $\boldsymbol{X}_0$ of the displacement vector is a point of intersection between the ray lines $\boldsymbol{X} - \boldsymbol{X}_{c(1)} = \boldsymbol{r}_{0(1)}\xi$ and $\boldsymbol{X} - \boldsymbol{X}_{c(2)} = \boldsymbol{r}_{0(2)}\xi$, where ξ is a parameter. To determine the point $\boldsymbol{X}_0$, we minimize the distance $d_{0(1-2)}$ of a point on the line $\boldsymbol{X} - \boldsymbol{X}_{c(1)} = \boldsymbol{r}_{0(1)}\xi$ to the line $\boldsymbol{X} - \boldsymbol{X}_{c(2)} = \boldsymbol{r}_{0(2)}\xi$, that is, $d_{0(1-2)}(\xi) = |(\boldsymbol{X}_{c(1)} + \boldsymbol{r}_{0(1)}\xi - \boldsymbol{X}_{c(2)}) \times \boldsymbol{r}_{0(2)}| \rightarrow \min$. When the minimal point $\xi_{0\min}$ is found, the endpoint $\boldsymbol{X}_0$ of the displacement vector is given by $\boldsymbol{X}_0 = \boldsymbol{X}_{c(1)} + \boldsymbol{r}_{0(1)}\xi_{0\min}$. Similarly, by minimizing the distance $d_{1(1-2)}$ of a point on the line $\boldsymbol{X} - \boldsymbol{X}_{c(1)} = r_{1(1)}\xi$ to the line $\boldsymbol{X} - \boldsymbol{X}_{c(2)} = \boldsymbol{r}_{1(2)}\xi$, that is, $d_{1(1-2)}(\xi) = |(\boldsymbol{X}_{c(1)} + \boldsymbol{r}_{1(1)}\xi - \boldsymbol{X}_{c(2)}) \times \boldsymbol{r}_{1(2)}| \rightarrow \min$, we can determine the other endpoint $\boldsymbol{X}_1 = \boldsymbol{X}_{c(1)} + \boldsymbol{r}_{1(1)}\xi_{1\min}$ of the displacement vector, where $\xi_{1\min}$ is the minimal point. Finally, the displacement vector $\boldsymbol{X}_1 - \boldsymbol{X}_0$ in the object space is recovered. The analysis for determining the displacement vector based on the perspective developable conical planes is intuitively simple. It will be pointed out in Sec. VI that the displacement vector can be directly determined using the composite image coordinates.

IV. Perspective Projection Under Surface Constraint

A. Correspondence Between Surface and Image Plane

Surface in the object space has the one-to-one correspondence to the image plane. The geometric relationship between the surface and the image plane is closely related to some applications in experimental aerodynamics, such as reconstruction of complex flow topology on surface from images of oil visualization and laser-sheet-induced fluorescence visualization. The surface could be a solid surface or a virtual surface like laser sheet. Consider a surface in the object space

$$X^3 = F(X^1, X^2) \tag{14}$$

When Eq. (14) is imposed as a surface constraint, the perspective projection transformation Eq. (7) becomes

$$\begin{aligned} w_{11}X^1 + w_{12}X^2 + w_{13}F(X^1, X^2) &= \boldsymbol{W}_1 \cdot \boldsymbol{X}_c \\ w_{21}X^1 + w_{22}X^2 + w_{23}F(X^1, X^2) &= \boldsymbol{W}_2 \cdot \boldsymbol{X}_c \end{aligned} \tag{15}$$

where $w_{ij}(i = 1, 2 \text{ and } j = 1, 2, 3)$ are the elements of the vectors $\boldsymbol{W}_1 = (w_{11}, w_{12}, w_{13})^T$ and $\boldsymbol{W}_2 = (w_{21}, w_{22}, w_{23})^T$. For the given surface $X^3 = F(X^1, X^2)$, the coordinates $(X^1, X^2)^T$ can be obtained from the image coordinates $\boldsymbol{x} = (x^1, x^2)^T$ by solving Eq. (15). Thus, the coordinates $\boldsymbol{X} = (X^1, X^2, X^3)^T$ in the object space can be symbolically expressed as a function of the image coordinates $\boldsymbol{x} = (x^1, x^2)^T$ by

$$\boldsymbol{X} = \boldsymbol{f}_s(\boldsymbol{x}) \tag{16}$$

In fact, Eq. (16) is a parametric representation of the surface using the image coordinates $\boldsymbol{x} = (x^1, x^2)^T$ as the parameters. Generally, the function $\boldsymbol{f}_s(\boldsymbol{x})$ cannot be written as a closed-form solution except for simple surfaces such as plane and cylindrical surface.

Differentiating Eq. (7), we have $\mathrm{d}\boldsymbol{W}_1 \cdot \boldsymbol{X} + \boldsymbol{W}_1 \cdot \mathrm{d}\boldsymbol{X} = \mathrm{d}\boldsymbol{W}_1 \cdot \boldsymbol{X}_c$ and $\mathrm{d}\boldsymbol{W}_2 \cdot \boldsymbol{X} + \boldsymbol{W}_2 \cdot \mathrm{d}\boldsymbol{X} = \mathrm{d}\boldsymbol{W}_2 \cdot \boldsymbol{X}_c$. For the fixed lens distortion terms, $\mathrm{d}\boldsymbol{W}_1 = \mathrm{d}x^1\boldsymbol{m}_3$, and $\mathrm{d}\boldsymbol{W}_2 = \mathrm{d}x^2\boldsymbol{m}_3$. Then, using $\mathrm{d}X^3 = (\partial F/\partial X^\beta)\mathrm{d}X^\beta(\beta = 1, 2)$, we have

$$\begin{pmatrix} \mathrm{d}X^1 \\ \mathrm{d}X^2 \end{pmatrix} = \boldsymbol{m}_3 \cdot (\boldsymbol{X}_c - \boldsymbol{f}_s)\boldsymbol{G}^{-1} \begin{pmatrix} \mathrm{d}x^1 \\ \mathrm{d}x^2 \end{pmatrix} \tag{17}$$

where

$$\boldsymbol{G} = \begin{pmatrix} w_{11} + w_{13}\partial F/\partial X^1 & W_{12} + w_{13}\partial F/\partial X^2 \\ w_{21} + w_{23}\partial F/\partial X^1 & w_{22} + w_{23}\partial F/\partial X^2 \end{pmatrix} \tag{18}$$

Furthermore, the differential $\mathrm{d}X^3 = (\partial F/\partial X^\beta)(\partial X^\beta/\partial x^\alpha)\,\mathrm{d}x^\alpha(\alpha = 1, 2; \beta = 1, 2)$ can be expressed as a function of the image coordinates $\mathrm{d}\boldsymbol{x} = (\mathrm{d}x^1, \mathrm{d}x^2)^T$. The fundamental relation between the differential $\mathrm{d}\boldsymbol{X}$ on the surface in the three-dimensional object space and $\mathrm{d}\boldsymbol{x}$ in the image plane is $\mathrm{d}\boldsymbol{X} = \bar{\boldsymbol{G}}\,\mathrm{d}\boldsymbol{x}$, where the 3×2 matrix $\bar{\boldsymbol{G}}$ is a function of the image coordinates, the camera parameters, and the geometric properties of the given surface. We know the first fundamental form of the surface $\mathrm{d}S^2 = |\mathrm{d}\boldsymbol{X}| = g_{\alpha\beta}\,\mathrm{d}x^\alpha\,\mathrm{d}x^\beta$, where the metric tensor is $g_{\alpha\beta} = (\partial\boldsymbol{X}/\partial x^\beta) \cdot (\partial\boldsymbol{X}/\partial x^\beta)(\alpha, \beta = 1, 2)$ and the image coordinates serve as the parametric variables. The first fundamental form allows us to measure the basic geometric quantities (arc length, area, and angle) on the surface.[20]

B. Motion Field Constrained on Surface

Following the discussion of the geometric relationship between a surface and the image plane, we consider the perspective projection of the motion field constrained on the surface. Consider a dynamical system

$$\frac{\mathrm{d}\boldsymbol{X}}{\mathrm{d}t} = \boldsymbol{U}(\boldsymbol{X}) \tag{19}$$

where $\boldsymbol{U}(\boldsymbol{X}) = (U_1, U_2, U_3)^T$ is the motion field in the three-dimensional object space and t is time. When the motion field is constrained on the nonpenetrating surface $X^3 = F(X^1, X^2)$, $\boldsymbol{U}(\boldsymbol{X})$ should be parallel to the surface, obeying $\boldsymbol{N} \cdot \boldsymbol{U}(\boldsymbol{X}) = 0$, where $\boldsymbol{N} = (-\partial F/\partial X^1, -\partial F/\partial X^2, 1)^T$ is the normal vector of the surface. Under the surface constraint, Eq. (19) is reduced to a two-dimensional system

$$\frac{\mathrm{d}}{\mathrm{d}t}\begin{pmatrix} X^1 \\ X^2 \end{pmatrix} = \begin{pmatrix} U_1[X^1, X^2, F(X^1, X^2)] \\ U_2[X^1, X^2, F(X^1, X^2)] \end{pmatrix} \tag{20}$$

Actually, Eq. (20) describes an orthographic projection of the motion field Eq. (19) onto the plane (X^1, X^2). According to Eqs. (16) and (17), the corresponding dynamical system in the image plane is

$$\boldsymbol{u} = \frac{\mathrm{d}}{\mathrm{d}t}\begin{pmatrix} x^1 \\ x^2 \end{pmatrix} = \frac{\boldsymbol{G}}{\boldsymbol{m}_3 \cdot (\boldsymbol{X}_c - \boldsymbol{f}_s)} \begin{pmatrix} U_1[\boldsymbol{f}_s(\boldsymbol{x})] \\ U_2[\boldsymbol{f}_s(\boldsymbol{x})] \end{pmatrix} \tag{21}$$

Here, we call $\boldsymbol{u} = \mathrm{d}\boldsymbol{x}/\mathrm{d}t = \mathrm{d}/\mathrm{d}t(x^1, x^2)^T$ the optical flow in the image plane. The optical flow, a term used in computer vision, is defined as the velocity field in the image plane that transforms one image into the next image in a time sequence. If Eq. (16) gives a one-to-one topological mapping (homeomorphism): $(x^1, x^2) \mapsto (X^1, X^2)$, the topological structure of the dynamical system Eq. (21) in the image plane is equivalent to that of Eq. (20) on the constrained surface when $\boldsymbol{G}$ has the full rank of two and $\boldsymbol{m}_3 \cdot (\boldsymbol{X}_c - \boldsymbol{f}_s)$ does not vanish. Once the optical flow $\boldsymbol{u} = \mathrm{d}\boldsymbol{x}/\mathrm{d}t$ is known, two components of the motion field $(U_1, U_2)^T$ can be determined from Eq. (21), and the third component U_3 is readily known from $\boldsymbol{N} \cdot \boldsymbol{U}(\boldsymbol{X}) = 0$ for a nonpenetrating surface.

The motion field $\boldsymbol{U}(\boldsymbol{X})$ is not specified so far, which could be a limiting viscous flowfield or an oil-film motion field driven by skin friction on surface. The physical constraints on for a specified $\boldsymbol{U}(\boldsymbol{X})$ can be used to reduce the number of unknowns. For instance, the incompressible flow obeys the continuity equation $\nabla \cdot \boldsymbol{U}(\boldsymbol{X}) = 0$, where $\nabla = (\partial/\partial X^1, \partial/\partial X^2, \partial/\partial X^3)^T$ is the Laplace operator. Differentiating $\boldsymbol{N} \cdot \boldsymbol{U}(\boldsymbol{X}) = 0$ with respect

to X^3, we have $\partial U_3/\partial X^3 = \partial U_\alpha/\partial X^3 \partial F/\partial X^\alpha$ $(\alpha = 1, 2)$. Substitution of this relation into $\nabla \cdot \boldsymbol{U}(\boldsymbol{X}) = 0$ yields a constraint on $(U_1, U_2)^T$ for the incompressible flow on a nonpenetrating surface, that is, $\partial U_\alpha/\partial X^\alpha + \partial U_\alpha/\partial X^3 \partial F/\partial X^\alpha = 0 (\alpha = 1, 2)$. In general, we seek a localized solution of Eq. (21) for $(U_1, U_2)^T$ in a sufficiently small domain rather than a global solution. In a neighborhood of a point $\boldsymbol{X}_0$, the motion field $(U_1, U_2)^T$ can be expanded as $U_i(\boldsymbol{X}) = e_{i0} + e_{i\alpha}(X^\alpha - X_0^\alpha)(i = 1, 2; \alpha = 1, 2, 3)$, where $e_{i0} = U_i(\boldsymbol{X}_0)$ are the local velocity components and $e_{i\alpha} = \partial U_i(\boldsymbol{X}_0)/\partial X^\alpha$ are the local deformation components that determine the local topological structures of the motion field near the critical points.[21] There are eight unknowns e_{i0} and e_{ij}. If flow is incompressible and irrotational where $\nabla \cdot \boldsymbol{U}(\boldsymbol{X}) = 0$ and $\nabla \times \boldsymbol{U}(\boldsymbol{X}) = 0$, eight unknowns are reduced to four unknowns after these constraints are imposed.

The preceding method for recovering the local motion field is, in principle, applicable to both discrete random particle patterns (e.g., particle-image-velocimetry patterns) and continuous passive scalar patterns (e.g., laser-sheet-induced fluorescence patterns). When discrete particle patterns are so coarse that an individual particle can be tracked, the local optical flow $\boldsymbol{u} = \mathrm{d}\boldsymbol{x}/\mathrm{d}t$ is the velocity of the particle in the image plane.[22,23] For dense discrete particle patterns, the local optical flow $\boldsymbol{u} = \mathrm{d}\boldsymbol{x}/\mathrm{d}t$ can be obtained using pattern correlation technique to seek the maximum correlation between two particle groups at two consecutive instants in the image plane. To recover the local optical flow $\boldsymbol{u} = \mathrm{d}\boldsymbol{x}/\mathrm{d}t$ for continuous passive scalar patterns, we need to consider the perspective projection of the transport equations of passive scalar through a specific imaging process. Generally, the perspective projection of transport process leads to the motion equations of the image intensity. The optical flow $\boldsymbol{u} = \mathrm{d}\boldsymbol{x}/\mathrm{d}t$ can be determined by solving the motion equation of the image intensity given the suitable boundary conditions and other constraints. Detailed discussion on the motion equations of the image intensity will be given in Sec. VII.

V. Correspondence Problem

In Sec. IV, after the surface constraint is imposed, three unknown coordinates in the object space are reduced to two, and the correspondence between the surface and the image plane is one to one. However, to determine three unknown coordinates from multiple views without any a priori constraint, the correspondence between two or more images is required for the same physical point in the object space. This is the point correspondence problem in three-dimensional vision. Experimental fluid dynamicists encounter this problem in particle-tracking velocimetry.

Longuet-Higgins[24] gave a relation between the corresponding points in two images. Consider two cameras in which the unit vectors $(\boldsymbol{m}_{1(n)}, \boldsymbol{m}_{2(n)}, \boldsymbol{m}_{3(n)})$ constitute a local right-hand coordinate system whose origin is located at the perspective center $\boldsymbol{X}_{c(n)}$, where the index $n = 1, 2$ denotes the cameras 1 and 2. The coordinates $\bar{\boldsymbol{X}}_{(n)} = (\bar{X}^1_{(n)}, \bar{X}^2_{(n)}, \bar{X}^3_{(n)})^T$ in the coordinate frames $(\boldsymbol{m}_{1(n)}, \boldsymbol{m}_{2(n)}, \boldsymbol{m}_{3(n)})$ are related by the translation and rotation transformation $\bar{X}^a_{(2)} = R_{\alpha\beta}(\bar{X}^\beta_{(1)} - T_r^\beta)$, where $\boldsymbol{R} = [R_{\alpha\beta}]$ and $\boldsymbol{T}_r = [T_r^\beta]$ are the rotation matrix and translation vector, respectively. A new matrix $\boldsymbol{Q}$ is given by $\boldsymbol{Q} = \boldsymbol{RS}$ or $S_{\alpha\beta} = R_{\alpha\mu} S_{\mu\beta}$, where $\boldsymbol{S}$ is the skew-symmetric matrix $S_{\mu\beta} = \varepsilon_{\mu\beta\sigma} T_r^\sigma$ and the permutation index $\varepsilon_{\mu\beta\sigma} = 1$, or -1, or 0 if (μ, β, σ) is an even, or odd permutation of (1, 2, 3), or otherwise. Thus, we know

$$\bar{X}^\alpha_{(2)} Q_{\alpha\beta} \bar{X}^\beta_{(1)} = R_{\alpha\kappa}\left(\bar{X}^\kappa_{(1)} - T_r^\kappa\right) R_{\alpha\mu} \varepsilon_{\mu\beta\sigma} T_r^\sigma \bar{X}^\beta_{(1)}$$

$$= \left(X^\mu_{(1)} - T_r^\mu\right) \varepsilon_{\mu\beta\sigma} T_r^\sigma \bar{X}^\beta_{(1)} = 0 \tag{22}$$

because the rotational matrix $\boldsymbol{R}$ is orthogonal $(R_{\alpha\mu} R_{\mu\beta} = \delta_{\alpha\beta})$ and $\varepsilon_{\mu\beta\sigma}$ is antisymmetric in every pair of its subscripts. When the image coordinates a $x^\alpha_{(n)}$ are relative to the principal point, the collinearity equations without lens distortion can be written as a simpler form $x^a_{(n)} = -c\bar{X}^\alpha_{(n)}/\bar{X}^3_{(n)}$, $(n = 1, 2; \alpha = 1, 2, 3)$. Dividing Eq. (22) by $\bar{X}^3_{(1)} \bar{X}^3_{(2)}/c^2$ yields the Longuet–Higgins equation for the point correspondence

$$x^\alpha_{(2)} Q_{\alpha\beta} x^\beta_{(1)} = 0 \tag{23}$$

where $\boldsymbol{Q}$ is the fundamental matrix related to the camera exterior orientation parameters. Given a sufficient number of point correspondences between two images, the elements $Q_{\alpha\beta}$ can be determined by solving the algebraic equations $(x^\alpha_{(2)} x^\beta_{(1)})_i Q_{\alpha\beta} = 0 (i \geq 8)$ using least-squares method.

The geometrical meaning of Eq. (23) is related to the epipolar lines in the image plane.[2,3] For a given point $(x^1_{(1)}, x^2_{(1)})$ in the image 1, its epipolar line in the image 2 is projection of a line connecting the object space point and the image point through the optical center of the camera 1 onto the image 2. This epipolar line in the image 2 is given by $x^\alpha_{(2)} p_{\alpha(1)} = 0$, where $p_{\alpha(1)} = Q_{\alpha\beta} x^\beta_{(1)}$ are the coefficients of the epipolar line. Thus, the fundamental matrix $\boldsymbol{Q}$ maps a point in image 1 to its epipolar line in image 2 and vice versa. Hence, Eq. (23) serves as the epipolar constraint to reduce the number of unknowns for establishing the point correspondence between images. When lens distortion exists, the epipolar constraint is $(x^\alpha_{(2)} + \delta x^\alpha_{(2)}) Q_{\alpha\beta} (x^\beta_{(1)} + \delta x^\beta_{(1)}) = 0$, where the lens distortion terms are $[\delta x^\alpha_{(n)}] = (\delta x^1_{(n)}, \delta x^2_{(n)}, 0)^T$. Because the lens distortion terms are nonlinear, an epipolar line is a curve rather than a straight line.

For two calibrated cameras, the correspondence between two images can be directly established from the collinearity equations. The collinearity equations (7) for cameras 1 and 2 are written as

$$\boldsymbol{W}_{1(n)} \cdot \left(\boldsymbol{X} - \boldsymbol{X}_{c(n)}\right) = 0, \qquad \boldsymbol{W}_{2(n)} \cdot \left(\boldsymbol{X} - \boldsymbol{X}_{c(n)}\right) = 0 \qquad (n = 1, 2) \tag{24}$$

Recombination of Eq. (24) yields two systems of linear equations for $\boldsymbol{X}$:

$$\boldsymbol{W}_{1\mathrm{com}} \boldsymbol{X} = \boldsymbol{B}_{1\mathrm{com}}, \qquad \boldsymbol{W}_{2\mathrm{com}} \boldsymbol{X} = \boldsymbol{B}_{2\mathrm{com}} \tag{25}$$

where the composite matrices and vectors are

$$\boldsymbol{W}_{1\mathrm{com}} = \begin{pmatrix} \boldsymbol{W}_{1(1)}{}^T \\ \boldsymbol{W}_{2(1)}{}^T \\ \boldsymbol{W}_{1(2)}{}^T \end{pmatrix}, \qquad \boldsymbol{W}_{2\mathrm{com}} = \begin{pmatrix} \boldsymbol{W}_{1(1)}{}^T \\ \boldsymbol{W}_{2(1)}{}^T \\ \boldsymbol{W}_{2(2)}{}^T \end{pmatrix}$$

$$\boldsymbol{B}_{1\mathrm{com}} = \begin{pmatrix} \boldsymbol{W}_{1(1)}{}^T \boldsymbol{X}_{c(1)} \\ \boldsymbol{W}_{2(1)}{}^T \boldsymbol{X}_{c(1)} \\ \boldsymbol{W}_{1(2)}{}^T \boldsymbol{X}_{c(2)} \end{pmatrix}, \qquad \boldsymbol{B}_{2\mathrm{com}} = \begin{pmatrix} \boldsymbol{W}_{1(1)}{}^T \boldsymbol{X}_{c(1)} \\ \boldsymbol{W}_{2(1)}{}^T \boldsymbol{X}_{c(1)} \\ \boldsymbol{W}_{2(2)}{}^T \boldsymbol{X}_{c(2)} \end{pmatrix} \tag{26}$$

Eliminating $\boldsymbol{X}$ from Eq. (25), we obtain a relation between the image coordinates $(x^1_{(1)}, x^2_{(1)})$ and $(x^1_{(2)}, x^2_{(2)})$, $\boldsymbol{G}(x^1_{(1)}, x^2_{(1)}; x^1_{(2)}, x^2_{(2)}) = \boldsymbol{W}_{1\mathrm{com}} \boldsymbol{W}^{-1}_{2\mathrm{com}} \boldsymbol{B}_{2\mathrm{com}} - \boldsymbol{B}_{1\mathrm{com}} = 0$. For a point $(x^1_{(1)}, x^2_{(1)})$ in image 1, its epipolar line in image 2 is given by minimizing the norm $\|\boldsymbol{G}(x^1_{(1)}, x^2_{(1)}; x^1_{(2)}, x^2_{(2)})\|$.

The Longuet–Higgins equation indicates that a point in image 1 corresponds to its epipolar line on image 2 and vice versa. Therefore, the point correspondence is not uniquely established between a pair of images because for a given image point $(x^1_{(1)}, x^2_{(1)})$ there is only one equation for two unknowns $(x^1_{(2)}, x^2_{(2)})$. To establish the point correspondence between images, at least four cameras (or four images) are needed. For four cameras or images, the Longuet–Higgins equations are $x^\alpha_{h(i)} Q_{\alpha\beta(i,j)} x^\beta_{h(j)} = 0$ $(i = 1, 2, 3, 4; j = 1, 2, 3, 4)$ where the subscript (i, j) denotes a pair of images. There are six pairs of images $(i, j) = (1, 2)$, (1,3), (1,4), (2,3), (2,4), and (3,4). Hence, for given $Q_{\alpha\beta(i,j)}$ and $(x^1_{(1)}, x^2_{(1)})$, we have a system of six quadratic equations for six unknowns $(x^1_{(2)}, x^2_{(2)}, x^1_{(3)}, x^2_{(3)}, x^1_{(4)}, x^2_{(4)})$. The solution can be found using an iterative method.

VI. Composite Image Space and Perspective Invariants

A. Composite Image Space

Once the point correspondence between two images is uniquely established, $\boldsymbol{W}_{1\mathrm{com}} \boldsymbol{X} = \boldsymbol{B}_{1\mathrm{com}}$ gives a relation between the object space coordinates $\boldsymbol{X}$ and the composite image coordinates $\boldsymbol{x}_{\mathrm{com}} = (x^1_{(1)}, x^2_{(1)}, x^1_{(2)})^T$. As shown in Fig. 6, the local coordinate frame $(\boldsymbol{m}_{1(1)}, \boldsymbol{m}_{2(1)}, \boldsymbol{m}_{3(1)})$ at the perspective center $\boldsymbol{X}_{c(1)}$ can serve as a frame for the composite image space in which $\boldsymbol{x}_{\mathrm{com}} = (x^1_{(1)}, x^2_{(1)}, x^1_{(2)})^T$ are the composite image coordinates along

the unit vectors $(\boldsymbol{m}_{1(1)}, \boldsymbol{m}_{2(1)}, \boldsymbol{m}_{3(1)})$. The coordinate $x^1_{(2)}$ of the corresponding point in image 2 is artificially assigned to the coordinate value in the axis $\boldsymbol{m}_{3(1)}$ in the composite image space. Thus, the lost dimension along the axis $\boldsymbol{m}_{3(1)}$ through projection in image 1 is recovered by using one coordinate value in image 2. Mapping between the composite image space and the object space is one to one. Differentiating $\boldsymbol{W}_{1\text{com}}\boldsymbol{X} = \boldsymbol{B}_{1\text{com}}$, we have $\boldsymbol{W}_{1\text{com}}\mathrm{d}\boldsymbol{X} + \mathrm{d}\boldsymbol{W}_{1\text{com}}\boldsymbol{X} = \mathrm{d}\boldsymbol{B}_{1\text{com}}$. Thus, a basic differential relation between the composite image space and object space is

$$\mathrm{d}\boldsymbol{X} = \boldsymbol{H}(\boldsymbol{x}_{\text{com}})\,\mathrm{d}\boldsymbol{x}_{\text{com}} \qquad \text{or} \qquad \mathrm{d}x^{\alpha} = H_{\alpha\beta}(\boldsymbol{x}_{\text{com}})\,\mathrm{d}x^{\beta}_{\text{com}} \tag{27}$$

where the matrix $\boldsymbol{H}(\boldsymbol{x}_{\text{com}})$ is

$$\boldsymbol{H}(\boldsymbol{x}_{\text{com}}) = \boldsymbol{W}^{-1}_{1\text{com}} \begin{pmatrix} \boldsymbol{m}^T_{(3)1}\left(\boldsymbol{W}^{-1}_{1\text{com}}\boldsymbol{B}_{1\text{com}} - \boldsymbol{X}_{c(1)}\right) & 0 & 0 \\ 0 & \boldsymbol{m}^T_{3(1)}\left(\boldsymbol{W}^{-1}_{1\text{com}}\boldsymbol{B}_{1\text{com}} - \boldsymbol{X}_{c(1)}\right) & 0 \\ 0 & 0 & \boldsymbol{m}^T_{3(2)}\left(\boldsymbol{W}^{-1}_{1\text{com}}\boldsymbol{B}_{1\text{com}} - \boldsymbol{X}_{c(2)}\right) \end{pmatrix} \tag{28}$$

Equation (27) can be used in stereoscopic particle image velocimetry to recover the displacement vector $\mathrm{d}\boldsymbol{X}$ from the displacement vector $\mathrm{d}\boldsymbol{x}_{\text{com}}$ in the composite image space. The geometric interpretation on stereoscopy of the displacement vector is given in Sec. III.C. The arc length $\mathrm{d}S$ of a three-dimensional curve in the object space is given by $\mathrm{d}S^2 = \mathrm{d}X^{\alpha}\mathrm{d}X^{\alpha} = H_{\mu\alpha}H_{\mu\beta}\mathrm{d}x^{\alpha}_{\text{com}}\mathrm{d}x^{\beta}_{\text{com}}$. Similarly, the tangent, curvature, and torsion of the curve can be also expressed as a function of the composite image space coordinates.

The motion field $U_{\alpha}(\boldsymbol{X}) = \mathrm{d}X^{\alpha}/\mathrm{d}t$ in the object space is related to the motion field $u_{\alpha}(\boldsymbol{x}_{\text{com}}) = \mathrm{d}x^{\alpha}_{\text{com}}/\mathrm{d}t$ in the composite image space by $U_{\alpha}(\boldsymbol{X}) = H_{\alpha\beta}(\boldsymbol{x}_{\text{com}})u_{\alpha}$. The motion field $U_{\alpha}(\boldsymbol{X})$ of a curve can be decomposed into two components, that is, $U_{\alpha}(\boldsymbol{X}) = \mathrm{d}X^{\alpha}[S(t), t]/\mathrm{d}t = \partial X^{\alpha}/\partial t + T^{\alpha}\mathrm{d}S/\mathrm{d}t$. The first term $\partial X^{\alpha}/\partial t$ is the apparent velocity of the curve, and the second is the deformation velocity along the curve. Similarly, the decomposition for $u_{\alpha}(\boldsymbol{x}_{\text{com}})$ is $u_{\alpha}(\boldsymbol{x}_{\text{com}}) = \mathrm{d}x^{\alpha}_{\text{com}}[s(t), t]/\mathrm{d}t = \partial x^{\alpha}_{\text{com}}/\partial t + t^{\alpha}_{\text{com}}\mathrm{d}s/\mathrm{d}t$. Additional physical constraints are required to determine the local deformation rate $\mathrm{d}s/\mathrm{d}t$ of the curve in the composite image space.

B. Perspective Invariants

The perspective invariants of a three-dimensional curve can be used to directly extract certain geometric features of the curve from images. Construction of algebraic and differential invariants of the curve is difficult because the perspective projection transformation is nonlinear. However, it is possible to construct semidifferential invariants in a special case of stereo image pair.[25] The perspective projection transformation for a pair of images is

$$\boldsymbol{x}_{h(i)} = \lambda_{(i)}\boldsymbol{P}_{h(i)}\boldsymbol{X}_h \qquad (i = 1, 2) \tag{29}$$

where $\boldsymbol{x}_{h(i)} = (x^1_{(i)}, x^2_{(i)}, 1)^T$ is the homogeneous image coordinates in a pair of images ($i = 1, 2$) and $\boldsymbol{P}_{h(i)}$ is a 3×4 matrix that depends only on the camera orientation parameters (see Sec. II). In general, because the scaling factors $\lambda_{(i)} = -c_{(i)}/\boldsymbol{m}_{3(i)} \cdot (\boldsymbol{X} - \boldsymbol{X}_{c(i)})$ for the two images are not the same, we cannot combine equations in Eq. (29) like a linear system of equations. Nevertheless, such combination is allowed under a special condition of $\lambda_{(1)} = \lambda_{(2)} = \lambda$ that implies $c_{(1)} = c_2$, $\boldsymbol{m}_{3(1)} = \boldsymbol{m}_{3(2)}$, and $\boldsymbol{m}_{3(1)} \cdot (\boldsymbol{X}_{c(2)} - \boldsymbol{X}_{c(1)}) = 0$. In fact, this indicates that these images have a relative shift on the same plane normal to the vector $\boldsymbol{m}_{3(1)} = \boldsymbol{m}_{3(2)}$ and two cameras are placed side by side and their optical axes are in parallel.

The preceding coplanar condition allows the combination of the collinearity equation (29) for the two images, making construction of the perspective invariants possible. The relationship between the composite image space and the object space for a three-dimensional curve is written as

$$\boldsymbol{x}_{\text{hcom}}[s(S)] = \lambda(S)\boldsymbol{P}_{\text{hcom}}\boldsymbol{X}_h \tag{30}$$

where $\boldsymbol{x}_{\text{hcom}} = (x^1_{(1)}, x^2_{(1)}, x^1_{(2)}, 1)^T$ are the composite homogeneous image coordinates, and $\boldsymbol{P}_{\text{hcom}}$ is a composite matrix from the elements of $\boldsymbol{P}_{h(1)}$ and $\boldsymbol{P}_{h(2)}$. The arc length S in the object space (X^1, X^2, X^3) is used as a parameter of the curve in Eq. (30). The arc length $s = s(S)$ in the composite image space $(x^1_{(1)}, x^2_{(1)}, x^1_{(2)})$ is a one-to-one function of S.

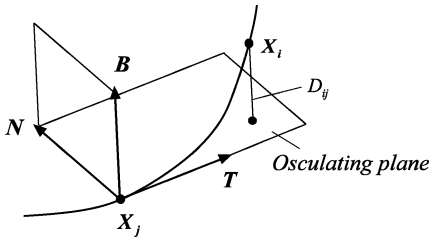

Fig. 7 Geometric meaning of the distance D_{ij}.

Brill et al.[25] have constructed projective invariants by differentiating Eq. (30) repeatedly with respect with S, arranging the results in matrix equations for several points on the curve, evaluating the determinants of the matrix equations, and then eliminating all of the factors related to the camera orientation parameters. We consider the curvatures in the composite image space and the object space $\kappa_{\text{im}} = |\ddot{\boldsymbol{x}}_{\text{com}}| = |\dot{\boldsymbol{x}}_{\text{com}} \times \ddot{\boldsymbol{x}}_{\text{com}}|$ and $\kappa_{\text{obj}} = |\ddot{\boldsymbol{X}}| = |\dot{\boldsymbol{X}} \times \ddot{\boldsymbol{X}}|$ (Ref. 20), where $\dot{\boldsymbol{x}}_{\text{com}} = \mathrm{d}\boldsymbol{x}_{\text{com}}/\mathrm{d}s$, $\ddot{\boldsymbol{x}}_{\text{com}} = \mathrm{d}^2\boldsymbol{x}_{\text{com}}/\mathrm{d}s^2$, $\dot{\boldsymbol{X}} = \mathrm{d}\boldsymbol{X}/\mathrm{d}S$, and $\ddot{\boldsymbol{X}} = \mathrm{d}^2\boldsymbol{X}/\mathrm{d}S^2$ are the derivatives with respect to the arc length. The torsions in the composite image space and the object space are $\tau_{im} = |\dot{\boldsymbol{x}}_{\text{com}}\ddot{\boldsymbol{x}}_{\text{com}}\dddot{\boldsymbol{x}}_{\text{com}}|/|\ddot{\boldsymbol{x}}_{\text{com}}|^2 = -|\dot{\boldsymbol{x}}_{\text{hcom}}\ddot{\boldsymbol{x}}_{\text{hcom}}\dddot{\boldsymbol{x}}_{\text{hcom}}|/|\ddot{\boldsymbol{x}}_{\text{com}}|^2$, and $\tau_{\text{obj}} = |\dot{\boldsymbol{X}}\ddot{\boldsymbol{X}}\dddot{\boldsymbol{X}}|/|\ddot{\boldsymbol{X}}|^2 = -|\dot{\boldsymbol{X}}_h\ddot{\boldsymbol{X}}_h\dddot{\boldsymbol{X}}_h|/|\ddot{\boldsymbol{X}}|^2$. These geometric quantities are expressed as the homogeneous coordinates $\boldsymbol{x}_{\text{hcom}} = (x^1_{(1)}, x^2_{(1)}, x^1_{(2)}, 1)^T$ and $\boldsymbol{X}_h = (X^1, X^2, X^3, 1)^T$ to utilize Eq. (30). Next, we define the distance D_{ij} from a point $\boldsymbol{X}_i$ to the osculating plane to the curve at the point $\boldsymbol{X}_j$, i.e., $D_{ij} = (\boldsymbol{X}_j - \boldsymbol{X}_i) \cdot \boldsymbol{B}_j = |(\boldsymbol{X}_j - \boldsymbol{X}_i)\dot{\boldsymbol{X}}_j\ddot{\boldsymbol{X}}_j|/\kappa_{\text{obj}}$, $j = |\boldsymbol{X}_{h,j}\,\dot{\boldsymbol{X}}_{h,j}\,\ddot{\boldsymbol{X}}_{h,j}\,\boldsymbol{X}_{h,i}|/\kappa_{\text{obj},j}$, where the subscripts i and j denote the quantities associated with the points $\boldsymbol{X}_i$ and $\boldsymbol{X}_j$, respectively. The geometrical meaning of D_{ij} is illustrated in Fig. 7. Similarly, in the composite image space the distance d_{ij} from a point $\boldsymbol{x}_{\text{com,i}}$ to the osculating plane to the curve at the point $\boldsymbol{x}_{\text{com},j}$ is $d_{ij} = |(\boldsymbol{x}_{\text{hcom},j} - \boldsymbol{x}_{\text{hcom},i})\,\dot{\boldsymbol{x}}_{\text{hcom},j}\,\ddot{\boldsymbol{x}}_{\text{hcom},j}|/\kappa_{\text{im},j} = |\boldsymbol{x}_{\text{hcom},j}\dot{\boldsymbol{x}}_{\text{hcom},j}\ddot{\boldsymbol{x}}_{\text{hcom},j}\boldsymbol{x}_{\text{hcom},i}|/\kappa_{\text{im},j}$. In addition, we introduce the following quantities $i(1, 1', 2, 3) = |\boldsymbol{x}_{\text{hcom},1}\,\dot{\boldsymbol{x}}_{\text{hcom},1}\,\boldsymbol{x}_{\text{hcom},2}\,\boldsymbol{x}_{\text{hcom},3}|$, $i(1, 2, 2', 3) = |\boldsymbol{x}_{\text{hcom},1}\,\boldsymbol{x}_{\text{hcom},2}\,\dot{\boldsymbol{x}}_{\text{hcom},2}\,\boldsymbol{x}_{\text{hcom},3}|$, $I(1, 1', 2, 3) = |\boldsymbol{X}_{h,1}\,\dot{\boldsymbol{X}}_{h,1}\,\boldsymbol{X}_{h,2}\,\boldsymbol{X}_{h,3}|$, and $I(1, 2, 2', 3) = |\boldsymbol{X}_{h,1}\,\boldsymbol{X}_{h,2}\,\dot{\boldsymbol{X}}_{h,2}\,\boldsymbol{X}_{h,3}|$ whose geometric meaning is not obvious. Differentiating Eq. (30) with respect to S and rearrangement yields several perspective invariants:

1) An invariant related to the torsions and the distances D_{ij} and d_{ij} is

$$\frac{\tau_{\text{im},1}d^2_{12}}{\tau_{\text{im},2}d^2_{21}} = \frac{\tau_{\text{obj},1}D^2_{12}}{\tau_{\text{obj},2}D^2_{21}} \tag{31}$$

For $\tau_{\text{obj},1} = 0$, $\tau_{\text{obj},2} \neq 0$, $D_{12} \neq 0$, and $D_{21} \neq 0$, then $\tau_{\text{im},1} = 0$. Therefore, the zero-torsion point of the curve in the object space corresponds to the zero-torsion point in the composite image space.

2) An invariant related to the curvatures, the distances D_{ij} and d_{ij}, and the quantities $i(1, 1', 2, 3)$, $i(1, 2, 2', 3)$, $I(1, 1', 2, 3)$, and $I(1, 2, 2', 3)$ is

$$\frac{\kappa_{\text{im},2}d_{12}i^2(1, 1', 2, 3)}{\kappa_{\text{im},1}d_{21}i^2(1, 2, 2', 3)} = \frac{\kappa_{\text{obj},2}D_{12}I^2(1, 1', 2, 3)}{\kappa_{\text{obj},1}D_{21}I^2(1, 2', 2, 3)} \tag{32}$$

For $\kappa_{\text{obj},2} = 0$, $\kappa_{\text{obj},1} \neq 0$, $D_{12} \neq 0$, and $D_{21} \neq 0$, then $\kappa_{\text{im},2} = 0$. The zero-curvature point of the curve in the object space corresponds to the zero-curvature point in the composite image space.

3) An invariant related to the distances D_{ij} and d_{ij} is

$$\frac{d_{21}d_{43}}{d_{41}d_{23}} = \frac{D_{21}D_{43}}{D_{41}D_{23}} \tag{33}$$

This result is analogous to the cross ratio of the distances on a line, the classical perspective invariant in perspective geometry.[2,26]

VII. Motion Equations of Image Intensity

A. General Consideration

Motion equations of the image intensity can be derived from underlying physical principles, which are solved to determine the optical flow from a time sequence of images of both continuous and discrete patterns. The image intensity $I(\boldsymbol{x}, t)$ is proportional to the radiance $L(\boldsymbol{X}, \boldsymbol{p}, \boldsymbol{q}, t)$ characterized by the physical parameters $\boldsymbol{p} = (p_1, p_2, \ldots, p_N)^T$ and the geometric parameters $\boldsymbol{q} = (q_1, q_2, \ldots, q_M)^T$ that is,

$$I(\boldsymbol{x}, t) = c_{\text{sys}} L(\boldsymbol{X}, \boldsymbol{p}, \boldsymbol{q}, t) \tag{34}$$

where c_{sys} is a coefficient related to the imaging system. Differentiating Eq. (34) with respect to time, we obtain the motion equation of the image intensity

$$\frac{\partial I}{\partial t} + \boldsymbol{u} \cdot \nabla_x I = c_{\text{sys}} \left(\frac{\partial L}{\partial t} + \boldsymbol{U} \cdot \nabla_X L + \frac{\mathrm{d}\boldsymbol{p}}{\mathrm{d}t} \cdot \nabla_p L + \frac{\mathrm{d}\boldsymbol{q}}{\mathrm{d}t} \cdot \nabla_q L \right) \tag{35}$$

where $\boldsymbol{u} = \mathrm{d}\boldsymbol{x}/\mathrm{d}t$ is the optical flow in the image plane, $\boldsymbol{U} = \mathrm{d}\boldsymbol{X}/\mathrm{d}t$ is the motion field in the object space, and the gradient operators are defined as $\nabla_x = (\partial/\partial x^1, \partial/\partial x^2)^T$, $\nabla_X = (\partial/\partial X^1, \partial/\partial X^2, \partial/\partial X^3)^T$, $\nabla_p = (\partial/\partial p_1, \ldots, \partial/\partial p_N)^T$, and $\nabla_q = (\partial/\partial q_1, \ldots, \partial/\partial q_N)^T$. The first term in the right-hand side of Eq. (35) is the local temporal change of the radiance, and the second term is the change induced by motion of an object in a nonhomogeneous radiance field. The third and fourth terms are associated with the changes of the physical and geometric parameters, respectively. Equation (35) is a generic form of the motion equation of the image intensity. A specific structure of Eq. (35) depends on a physical process being studied.

To determine the optical flow, Horn and Schunck[27] suggested the brightness constraint equation $\partial I/\partial t + \boldsymbol{u} \cdot \nabla_x I = 0$ in computer vision. In fact, the brightness constraint equation assumes that the image intensity remains invariant along a stream of images. In general, this assumption, which is not related to any physical process, does not hold exactly.[28] Even for a moving Lambertian surface, the right-hand side in Eq. (35) does not vanish. In the following subsections, we derive the motion equations of the image intensity for typical transport processes of passive scalar and density-varying flows. In principle, the optical flow can be determined by solving the motion equation of the image intensity as a constrained variational problem.

B. Emitting Passive Scalar Transport

We consider a transport process of passive scalar emitting radiation of a certain wavelength such as fluorescent dye in fluids. The radiance from the emitting scalar is assumed to be proportional to the density or concentration $\psi(\boldsymbol{X}, t)$ of the scalar $L(\boldsymbol{X}, t) = c_\psi \psi(\boldsymbol{X}, t)$ where c_ψ is a constant coefficient. The density of the scalar $\psi(\boldsymbol{X}, t)$ obeys the transport equation

$$\frac{\mathrm{d}\psi}{\mathrm{d}t} = \frac{\partial \psi}{\partial t} + \boldsymbol{U} \cdot \nabla \psi = D_\psi \nabla_X^2 \psi \tag{36}$$

where D_ψ is the diffusion coefficient of the scalar. Differentiating Eq. (34) and using Eq. (36), we have the rate of change of the image intensity

$$\frac{\mathrm{d}I(\boldsymbol{x}, t)}{\mathrm{d}t} = D_\psi \nabla_X^2 I(\boldsymbol{x}, t) \tag{37}$$

The Laplace operator ∇_X^2 can be expressed in the image coordinates $\boldsymbol{x}$ as $\nabla_X^2 = h_\gamma \partial/\partial x^\gamma + h_{\gamma\alpha} \partial^2/\partial x^\alpha \partial x^\gamma$, where h_λ and $h_{\lambda\alpha}$ are defined as $h_\gamma = \partial^2 x^\gamma / \partial X^\beta \partial X^\beta$ and $h_{\gamma\alpha} = \partial x^\gamma / \partial X^\beta \partial x^\alpha / \partial X^\beta$ ($\alpha = 1, 2$; $\gamma = 1, 2$; $\beta = 1, 2, 3$). For a calibrated camera, h_γ and $h_{\gamma\alpha}$ are calculated by using the collinearity equations from the image coordinates when a constrained surface $X^3 = F(X^1, X^2)$ like a planar laser sheet is imposed (see Sec. IV). Thus, the motion equation of the image intensity for a passive scalar transport process is

$$\frac{\partial I}{\partial t} + u_\alpha \frac{\partial I}{\partial x^\alpha} = D_\psi \left(h_\gamma \frac{\partial I}{\partial x^\gamma} + h_{\gamma\alpha} \frac{\partial^2 I}{\partial x^\alpha \partial x^\gamma} \right) \tag{38}$$

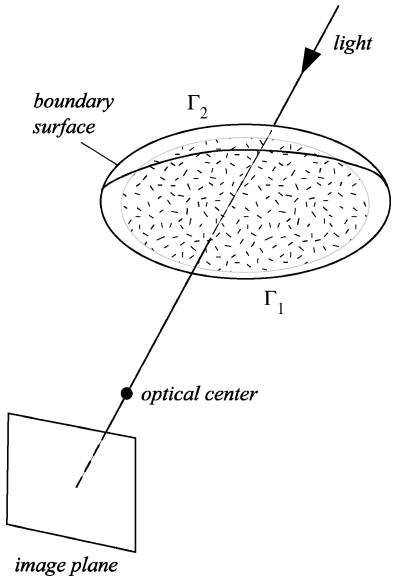

Fig. 8 Transmittance of a light ray through passive scalar.

In a special case of the orthographic projection $x^\alpha = X^\alpha$, we know $h_\gamma = 0$ and $h_{\gamma\alpha} = \delta_{\gamma\alpha}$. Thus, Eq. (38) is reduced to the standard diffusion equation

$$\frac{\partial I}{\partial t} + u_\alpha \frac{\partial I}{\partial x^\alpha} = D_\psi \left(\frac{\partial^2 I}{\partial x^\alpha \partial x^\alpha} \right) \tag{39}$$

When the optical flow u_α is obtained by solving Eq. (38), the motion field on the constrained surface in the object space can be determined from Eq. (21). If the constrained surface is a plane like a planar laser sheet, the perspective projection between the image plane and the constrained plane is simple. Particularly, when the image plane is parallel to the constrained plane, the optical flow is proportional to the two-dimensional motion field on the constrained plane.

C. Transmittant Passive Scalar Transport

The motion equation of the image intensity is derived for transmittant passive scalar transport in fluid flow. When a light ray transmits through a bulk of passive scalar, as shown in Fig. 8, the intensity of light at certain wavelength is attenuated as a result of absorption and scattering by the scalar. It is assumed that absorption and scattering by fluid are negligible and the scalar does not change the density of fluid. The radiance reaching a camera through the scalar is

$$L = L_0 \exp\left(-\int_0^s \beta_{\text{ext}} \, \mathrm{d}s \right) \tag{40}$$

where $\boldsymbol{s}$ is the path vector and β_{ext} is the extinction coefficient. Consider a bulk of the participating passive scalar confined by two boundary surfaces Γ_1 and Γ_2, as shown in Fig. 8. We assume that the camera is far enough away from the bulk of scalar such that the light path is almost parallel to the optical axis, that is, $\boldsymbol{s} \approx -\boldsymbol{m}_3$. In this case, it is convenient to use the object space coordinates $\bar{X}^i = m_{i_\alpha}(X^\alpha - X_c^\alpha)(i = 1, 2, 3)$ in the local orthogonal frame $(\boldsymbol{m}_1, \boldsymbol{m}_2, \boldsymbol{m}_3)$, where $m_{\beta\alpha} m_{\gamma\alpha} = \delta_{\gamma\beta}$. Under the preceding conditions, the transmittant radiance in Eq. (40) can be written as

$$L(\bar{\boldsymbol{X}}, t) = L_0 \exp\left[-\int_{\Gamma_1}^{\Gamma_2} \beta_{\text{ext}}(\bar{\boldsymbol{X}}, t) \, \mathrm{d}\bar{X}^3 \right] \tag{41}$$

where the boundary surfaces are $\bar{X}^3 = \Gamma_1(\bar{X}^1, \bar{X}^2, t)$ and $\bar{X}^3 = \Gamma_2(\bar{X}^1, \bar{X}^2, t)$. Here we generally consider the time-dependent boundaries even through the boundaries are usually fixed in applications. The extinction coefficient is proportional to the concentration $\psi(\bar{\boldsymbol{X}}, t)$ of the scalar, that is, $\beta_{\text{ext}}(\bar{\boldsymbol{X}}, t) = \varepsilon_\psi \psi(\bar{\boldsymbol{X}}, t)$, where ε_ψ is an

absorption coefficient. The relationship between the image intensity and the radiance is $I(\boldsymbol{x}, t) = c_{\text{sys}} L(\bar{\boldsymbol{X}}, t)$, where $\boldsymbol{x} = (x^1, x^2)^T$ is the image coordinates. Combination of these relations with Eq. (41) leads to

$$I(\boldsymbol{x}, t) = c_{\text{sys}}\, L_0 \exp\left[-\varepsilon_\psi \int_{\Gamma_1}^{\Gamma_2} \psi(\bar{\boldsymbol{X}}, t)\, \mathrm{d}\bar{X}^3\right] \tag{42}$$

Differentiating Eq. (42) with respect to time, we have

$$\frac{\mathrm{d}I(\boldsymbol{x}, t)}{\mathrm{d}t} = -\varepsilon_\psi I(\boldsymbol{x}, t)\left(\int_{\Gamma_1}^{\Gamma 2} \frac{\mathrm{d}\psi}{\mathrm{d}t}\, \mathrm{d}\bar{X}^3 + \psi\Big|_{\Gamma_2} \frac{\mathrm{d}\Gamma_2}{\mathrm{d}t} - \psi\Big|_{\Gamma_1} \frac{\mathrm{d}\Gamma_1}{\mathrm{d}t}\right) \tag{43}$$

Because $\psi(\boldsymbol{X}, t)$ obeys the transport equation (36), the first term in the right-hand side of Eq. (43) is

$$\int_{\Gamma_1}^{\Gamma_2} \frac{\mathrm{d}\psi}{\mathrm{d}t}\, \mathrm{d}\bar{X}^3 = D_\psi \int_{\Gamma_1}^{\Gamma_2} \frac{\partial^2 \psi}{\partial X^\alpha \partial X^\alpha}\, \mathrm{d}\bar{X}^3 = D_\psi \int_{\Gamma_1}^{\Gamma_2} \frac{\partial^2 \psi}{\partial \bar{X}^\alpha \partial \bar{X}^\alpha}\, \mathrm{d}\bar{X}^3 \qquad (\alpha = 1, 2, 3) \tag{44}$$

Integration by parts yields

$$\int_{\Gamma_1}^{\Gamma_2} \frac{\partial^2 \psi}{\partial \bar{X}^\alpha \partial \bar{X}^\alpha}\, \mathrm{d}\bar{X}^3 = \frac{\partial^2}{\partial \bar{X}^\beta \partial \bar{X}^\beta} \int_{\Gamma_1}^{\Gamma_2} \psi\, \mathrm{d}\bar{X}^3 + \text{B.T.} \qquad (\beta = 1, 2; \alpha = 1, 2, 3) \tag{45}$$

where B.T. denotes the boundary terms containing the values of $\psi(\boldsymbol{X}, t)$ and its derivatives on the boundary surfaces. We consider that a bulk of the passive scalar is confined in a domain outside, which $\psi(\bar{\boldsymbol{X}}, t)$ and its derivatives rapidly decrease zero. This represents a typical case in applications. For example, the boundaries are windows of the test section of a wind tunnel or water tunnel. Therefore, when the boundary surfaces Γ_1 and Γ_2 are so large that the boundary terms vanish, Eq. (43) becomes

$$\frac{\mathrm{d}I(\boldsymbol{x}, t)}{\mathrm{d}t} = -\varepsilon_\psi D_\psi I(\boldsymbol{x}, t) \frac{\partial^2}{\partial \bar{X}^\beta \partial \bar{X}^\beta} \int_{\Gamma_1}^{\Gamma_2} \psi\, \mathrm{d}\bar{X}^3 \qquad (\beta = 1, 2) \tag{46}$$

Using the perspective projection transformation $x^\beta - x_p^\beta = -c\bar{X}^\beta/\bar{X}^3$ $(\beta = 1, 2)$, we express the Laplace operator as $\partial^2/\partial \bar{X}^\beta \partial \bar{X}^\beta = \lambda^2 \partial^2/\partial x^\beta \partial x^\beta$ $(\beta = 1, 2)$, where $\lambda = -c/\bar{X}^3$ is the scaling factor. Replacing $\psi(\bar{\boldsymbol{X}}, t)$ by $I(\boldsymbol{x}, t)$ in Eq. (46), we obtain the motion equation of the image intensity for transmittance images of the transported passive scalar

$$\frac{\partial I}{\partial t} + u_\beta \frac{\partial I}{\partial x^\beta} = D\psi \lambda^2 \left(\frac{\partial^2 I}{\partial x^\beta \partial x^\beta} - I^{-1} \frac{\partial I}{\partial x^\beta} \frac{\partial I}{\partial x^\beta}\right) \qquad (\beta = 1, 2) \tag{47}$$

For a given boundary surface $\bar{X}^3 = \Gamma_1(\bar{X}^1, \bar{X}^2)$, facing the camera there is a one-to-one mapping between the surface and the image plane, and therefore the scaling factor $\lambda = -c/\bar{X}^3$ can be expressed in the image coordinates $\boldsymbol{x} = (x^1, x^2)^T$. In many applications, the boundary is a plane window of the test section such that the scaling factor is approximately a ratio between the principal distance of the camera and the distance of the camera to the window.

After the optical flow u_α is determined by solving Eq. (47), we want to recover the motion field in the object space. For the incompressible flow bounded by the fixed boundary surfaces Γ_1 and Γ_2, Eq. (43) is written as

$$\frac{\mathrm{d}I}{\mathrm{d}t} = -\varepsilon_\psi I \left(\int_{\Gamma_1}^{\Gamma_2} \frac{\partial \psi}{\partial t}\, \mathrm{d}\bar{X}^3 + \int_{\Gamma_1}^{\Gamma_2} \nabla \cdot (\psi \boldsymbol{U})\, \mathrm{d}\bar{X}^3\right) \tag{48}$$

The second term in the right-hand side of Eq. (48) can be decomposed into

$$\int_{\Gamma_1}^{\Gamma_2} \nabla \cdot (\psi \boldsymbol{U})\, \mathrm{d}\bar{X}^3 = \nabla_{12} \cdot \int_{\Gamma_1}^{\Gamma_2} \psi \boldsymbol{U}_{12}\, \mathrm{d}\bar{X}^3 - \boldsymbol{N} \cdot (\psi \boldsymbol{U})\Big|_{\Gamma_1}^{\Gamma_2} \tag{49}$$

where the gradient operator ∇_{12} is defined as $\nabla_{12} = (\partial/\partial \bar{X}^1, \partial/\partial \bar{X}^2)^T$, the two-dimensional velocity $\boldsymbol{U}_{12}$ is $\boldsymbol{U}_{12} = (U_1, U_2)^T$, and $\boldsymbol{N} = (-\partial \bar{X}_3/\partial \bar{X}_1, -\partial \bar{X}_3/\partial \bar{X}_2, 1)^T$ is the normal vector of the boundary surfaces Γ_1 and Γ_2. Then, we introduce the average velocity in terms of the scalar $\psi(\bar{\boldsymbol{X}}, t)$:

$$\langle \boldsymbol{U}_{12} \rangle_\psi = \frac{\int_{\Gamma_1}^{\Gamma_2} \psi \boldsymbol{U}_{12}\, \mathrm{d}\bar{X}^3}{\int_{\Gamma_1}^{\Gamma_2} \psi\, \mathrm{d}\bar{X}^3} \tag{50}$$

Assuming zero flux $\boldsymbol{N} \cdot (\psi \boldsymbol{U}) = 0$ at the boundary surfaces and combining Eq. (48) with Eqs. (49), (50), and (42), we obtain

$$u_\alpha \frac{\partial I}{\partial x^\alpha} = \langle \boldsymbol{U}_{12} \rangle_\psi \cdot \nabla_{12} I + I \ell n \left(\frac{I}{c_{\text{sys}} L_0}\right) \nabla_{12} \cdot \langle \boldsymbol{U}_{12} \rangle_\psi \tag{51}$$

When the flow is nearly two dimensional between two plane boundaries (windows) such that $\nabla_{12} \cdot \langle \boldsymbol{U}_{12} \rangle_\psi \approx 0$, Eq. (51) is simplified to

$$u_\alpha \frac{\partial I}{\partial x^\alpha} = \langle \boldsymbol{U}_{12} \rangle_\psi \cdot \nabla_{12} I \tag{52}$$

Thus, the average velocity $\langle \boldsymbol{U}_{12} \rangle_\psi$ can be recovered from the optical flow $\boldsymbol{u} = (u_1, u_2)^T$. In particular, when the image plane is parallel to the plane boundary Γ_1 the optical flow $\boldsymbol{u}$ is simply proportional to the average velocity $\langle \boldsymbol{U}_{12} \rangle_\psi$.

D. Schlieren Image of Density-Varying Flow

The schlieren technique has been widely used for flow visualization of density-varying flows such as compressible flows and natural convection flows. The image intensity I in a schlieren image depends on the gradient of the fluid density ρ by the following relation[29]:

$$\frac{I - I_K}{I_K} = C_{\text{schl}} \int_{\Gamma_1}^{\Gamma_2} \frac{\partial \rho}{\partial X^2}\, \mathrm{d}X^3 \tag{53}$$

where I_k is the reference image intensity with the knife edge inserted in the focal plane when no variation of the density exists in the test section and c_{schl} is a coefficient related to setting of the schlieren system. Figure 9 shows the coordinate system and the boundary surfaces $X^3 = \Gamma_1(X^1, X^2)$ and $X^3 = \Gamma_2(X^1, X^2)$, which a light ray passes through. The knife edge is set to be normal to the gradient of the fluid density $\partial \rho/\partial X^2$. The image intensity $\boldsymbol{I}$ is a function of the image coordinates $\boldsymbol{x} = (x^1, x^2)^T$, which is related to the object space coordinates $\boldsymbol{X} = (X^1, X^2, X^3)^T$ by the perspective projection transformation. On the constrained surface $X^3 = \Gamma_2(X^1, X^2)$, there is a one-to-one mapping between $\boldsymbol{x}$ and $\boldsymbol{X}$.

Taking partial differentiation with respect to time in Eq. (53) and using the continuity equation $\partial \rho/\partial t + \nabla \cdot (\rho \boldsymbol{U}) = 0$, we have

$$-\frac{\partial I}{\partial t} = I_K C_{\text{schl}} \int_{\Gamma_1}^{\Gamma_2} \frac{\partial}{\partial X^2} [\nabla \cdot (\rho \boldsymbol{U})]\, \mathrm{d}X^3 \tag{54}$$

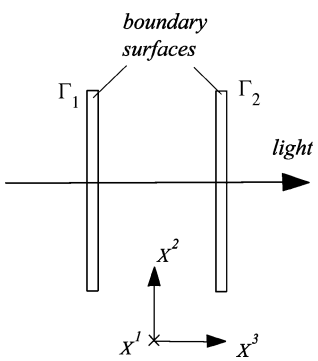

Fig. 9 Transmittance of a light ray through density-varying medium.

Integration by parts leads to

$$\int_{\Gamma_1}^{\Gamma_2} \frac{\partial}{\partial X^2}[\nabla\cdot(\rho\boldsymbol{U})]\,\mathrm{d}X^3 = \frac{\partial}{\partial X^2}\int_{\Gamma_1}^{\Gamma_2} \nabla\cdot(\rho\boldsymbol{U})\,\mathrm{d}X^3 - \nabla\cdot(\rho\boldsymbol{U})\frac{\partial X^3}{\partial X^2}\bigg|_{X^3=\Gamma_1}^{X^3=\Gamma_2} \tag{55}$$

The integral in the first term in the right-hand side of Eq. (55) can be decomposed into

$$\int_{\Gamma_1}^{\Gamma_2} \nabla\cdot(\rho\boldsymbol{U})\,\mathrm{d}X^3 = \nabla_{12}\cdot\int_{\Gamma_1}^{\Gamma_2}\rho\boldsymbol{U}_{12}\,\mathrm{d}X^3 - \boldsymbol{N}\cdot(\rho\boldsymbol{U})|_{\Gamma_1}^{\Gamma_2} \tag{56}$$

where $\nabla_{12}=(\partial/\partial X^1, \partial/\partial X^2)^T$, $\boldsymbol{U}_{12}=(U_1, U_2)^T$, and $\boldsymbol{N}=(-\partial X_3/\partial X_1, -\partial X_3/\partial X_2, 1)^T$.

Define the average velocity in terms of the density ρ:

$$\langle\boldsymbol{U}_{12}\rangle_\rho = \frac{\int_{\Gamma_1}^{\Gamma_2}\rho\boldsymbol{U}_{12}\,\mathrm{d}\bar{X}^3}{\int_{\Gamma_1}^{\Gamma_2}\rho\,\mathrm{d}\bar{X}^3} \tag{57}$$

Also, from Eq. (53), we know

$$\int_{\Gamma_1}^{\Gamma_2}\rho\,\mathrm{d}X^3 = \frac{I}{I_K C_{\mathrm{schl}}}\int_{X_0^2}^{X^2}(I-I_k)\,\mathrm{d}X^2 + \int_{X_0^2}^{X^2}\rho\frac{\partial X^3}{\partial X^2}\bigg|_{X^3=\Gamma_1}^{X^3=\Gamma_2}\mathrm{d}X^2 \tag{58}$$

where X_0^2 is a fixed point in X^2. For two nonpenetrating plane surfaces $X^3=\Gamma_1=\text{const}$ and $X^3=\Gamma_2=\text{const}$, where $N\cdot(\rho\boldsymbol{U})=0$, using Eqs. (54–58), we obtain a conservation form of equation

$$\frac{\partial}{\partial t}\int_{X_0^2}^{X^2}(I-I_k)\,\mathrm{d}X^2 + \nabla_{12}\cdot\left[\langle\boldsymbol{U}_{12}\rangle_\rho\int_{X_0^2}^{X^2}(I-I_k)\,\mathrm{d}X^2\right]=0 \tag{59}$$

The image coordinates $\boldsymbol{x}$ in the image intensity I can be uniquely converted to the object space coordinates $\boldsymbol{X}$ on the constrained plane $X^3=\Gamma_2=\text{const}$ through the perspective projection transformation. Therefore, from a time sequence of schlieren images the average velocity $\langle\boldsymbol{U}_{12}\rangle_\rho$ can be determined by solving Eq. (59). Note that Eq. (59) is also valid for two-phase flows when ρ is interpreted as the mean density in terms of the volume fraction.

E. Shadowgraph Image of Density-Varying Flow

In contrast to a schlieren image, the image intensity I in a shadowgraph image depends on the second derivative of the fluid density ρ, that is (Ref. 29),

$$\frac{I-I_T}{I_T} = C_{\mathrm{shad}}\int_{\Gamma_1}^{\Gamma_2}\nabla_{12}^2\,\rho\,\mathrm{d}X^3 \tag{60}$$

where I_T is the initial image intensity, C_{shad} is a coefficient related to setting of the shadowgraph system, and ∇_{12}^2 is the Laplace operator in the (X^1, X^2) plane. For simplicity, we consider the nonpenetrating plane surfaces $X^3=\Gamma_1=\text{const}$ and $X^3=\Gamma_2=\text{const}$, where $\boldsymbol{N}\cdot(\rho\boldsymbol{U})=0$. Taking partial differentiation with respect to time in Eq. (60), and using the continuity equation $\partial\rho/\partial t+\nabla\cdot(\rho\boldsymbol{U})=0$ and the relation Eq. (56), we have

$$-\frac{I}{I_T C_{\mathrm{shad}}}\frac{\partial I}{\partial t} = \nabla_{12}^2\cdot\left[\nabla_{12}\cdot\int_{\Gamma_1}^{\Gamma_2}\rho\boldsymbol{U}_{12}\,\mathrm{d}X^3\right] \tag{61}$$

From Eq. (60), we obtain the integral of the density

$$\int_{\Gamma_1}^{\Gamma_2}\rho\,\mathrm{d}X^3 = \frac{I}{I_T C_{\mathrm{shad}}}\nabla_{12}^{-2}(I-I_T) \tag{62}$$

where $\nabla_{12}^{-2}(I-I_T)$ is the symbolic expression of a solution of the Poisson equation $\nabla_{12}^2\phi = I-I_T$. Use of Eqs. (57) and (62) yields a conservation form of equation

$$\frac{\partial}{\partial t}\nabla_{12}^{-2}(I-I_T) + \nabla_{12}\cdot\left[\langle\boldsymbol{U}_{12}\rangle_\rho\nabla_{12}^{-2}(I-I_T)\right]=0 \tag{63}$$

F. Transmittance Image of Density-Varying Flow

For certain imaging system like a collimated monochromatic x-ray system, the image intensity I in a transmittance image depends on the fluid density ρ (Ref. 30):

$$\frac{I-I_T}{I_T} = C_{\mathrm{trans}}\int_{\Gamma_1}^{\Gamma_2}\rho\,\mathrm{d}X^3 \tag{64}$$

where I_T is the initial image intensity and C_{trans} is a coefficient related to setting of the imaging system. For the plane surfaces with zero mass flux, using the similar techniques described before, we obtain

$$\frac{\partial}{\partial t}(I-I_T) + \nabla_{12}\cdot[\langle\boldsymbol{U}_{12}\rangle_\rho(I-I_T)]=0 \tag{65}$$

VIII. Conclusions

The general principles and methodologies have been developed for quantitative image-based measurements of the geometric and kinematic properties of deformable bodies like fluids. Several formulations of the perspective projection transformation from the object space to the image plane are described, which are selectively used depending on its convenience for a specific problem. The perspective developable conical surface containing a three-dimensional curve is constructed, which provides a general means to determine a three-dimensional curve and the displacement vector in the object space from images. The perspective projection transformation under the surface constraint allows one-to-one mapping between the surface and the image plane. Hence, the geometric properties and motion field on the constrained surface and the image plane are uniquely related. The correspondence problem between multiple images is discussed for recovery of three-dimensional geometry and motion. The concept of the composite image space is introduced, and its geometric connection with the object space is established. In a special composite image space, several perspective invariants of a three-dimensional curve are constructed, allowing direct extraction of certain geometric properties of the curve from images. The motion equations of the image intensity are derived for emitting passive scalar transport, transmittant passive scalar transport, and schlieren, shadowgraph, and transmittance images of density-varying flows. These equations provide a rational foundation for recovering the optical flow and the corresponding motion field of fluid flows from a time sequence of images of continuous and discrete patterns.

References

[1]Mikhail, E. M., Bethel, J. S., and McGlone, J. C., *Introduction to Modern Photogrammetry*, Wiley, New York, 2001.

[2]Mundy, J. L., and Zisserman, A.,"Projective Geometry for Machine Vision," *Geometric Invariance in Computer Vision*, edited by J. Mundy and A. Zisserman, MIT Press, Cambridge, MA, 1992.

[3]Faugeras, O., *Three-Dimensional Computer Vision*, MIT Press, Cambridge, MA, 1993.

[4]Cipolla, R., and Giblin, P., *Visual Motion of Curves and Surfaces*, Cambridge Univ. Press, 2000.

[5]Ritter, G. X., and Wilson, J. N., *Handbook of Computer Vision Algorithms in Image Algebra*, CRC Press, Boca Raton, FL, 1996.

[6]McGlone, J. C.,"Analytic Data-Reduction Schemes in Non-Topographic Photogrammetry," *Non-Topographic Photogrammetry*, 2nd ed., edited by H. M. Karara, American Society for Photogrammetry and Remote Sensing, Falls Church, VA, 1989, Chap. 4, pp. 37–55.

[7]Wong, K. W., "Basic Mathematics of Photogrammetry," *Manual of Photogrammetry*, 4th ed., edited by C. C. Slama, American Society of Photogrammetry, Falls Church, VA, 1980, Chap. 2, pp. 37–101.

[8]Wolf, P., *Elements of Photogrammetry*, McGraw–Hill, New York, 1983, pp. 559–601.

[9]Fraser, C. S., "Photogrammetric Camera Component Calibration—A Review of Analytical Techniques," *Calibration and Orientation of Cameras in Computer Vision*, edited by A. Gruen and T. S. Huang, Springer-Verlag, Berlin, 2001, Chap. 4.

[10]Gruen, A., and Huang, T. S., *Calibration and Orientation of Cameras in Computer Vision*, Springer-Verlag, Berlin, 2001.

[11]Liu, T., Cattafesta, L. N., Radeztsky, R. H., and Burner, A. W., "Photogrammetry Applied to Wind-Tunnel Testing," *AIAA Journal*, Vol. 38, No. 6, 2000, pp. 964–971.

[12]Fraser, C. S., "Optimization of Networks in Non-Topographic Photogrammetry," *Non-Topographic Photogrammetry*, 2nd ed., edited by H. M. Karara, American Society for Photogrammetry and Remote Sensing, Falls Church, VA, 1989, pp. 95–106.

[13]Abdel-Aziz, Y. I., and Karara, H. M., "Direct Linear Transformation from Comparator Coordinates into Object Space Coordinates in Close-Range Photogrammetry," *Proceedings of the ASP/UI Symposium on Close-Range Photogrammetry*, Univ. of Illinois, Urbana, IL, 1971, pp. 1–18.

[14]Tsai, R. Y., "A Versatile Camera Calibration Technique for High-Accuracy 3D Machine Vision Metrology Using Off-the-Shelf TV Cameras and Lenses," *IEEE Journal of Robotics and Automation*, Vol. RA-3, No. 4, 1987, pp. 323–344.

[15]Struik, D. J., *Lectures on Classical Differential Geometry*, 2nd ed., Dover, New York, 1961, Chap. 2.

[16]Batchelor, G. K., *An Introduction to Fluid Mechanics*, Cambridge Univ. Press, Cambridge, England, U.K., 1988, Chap. 2.

[17]Betchov, R., "On the Curvature and Torsion of an Isolated Vortex Filament," *Journal of Fluid Mechanics*, Vol. 22, Pt. 3, 1965, pp. 471–479.

[18]Arroyo, M. P., and Greated, C. A., "Stereoscopic Particle Image Velocimetry," *Measurement Science Technology*, Vol. 2, No. 12, 1991, pp. 1181–1186.

[19]Prasad, A. K., and Adrian, R. J., "Stereoscopic Particle Image Velocimetry Applied to Liquid Flows," *Experiments in Fluids*, Vol. 15, No. 1, 1993, pp. 49–60.

[20]Kreyszig, E., *Differential Geometry*, Dover, New York, 1991, Chap. 3.

[21]Bakker, P. G., *Bifurcations in Flow Patterns*, Kluwer Academic, Norwell, MA, 1991, Chap. 1.

[22]Dracos, T., and Gruen, A., "Videogrammetric Methods in Velocimetry," *Applied Mechanics Reviews*, Vol. 51, No. 6, 1998, pp. 387–413.

[23]Maas, H. G., Gruen, A., and Papantoniou, D., "Particle Tracking Velocimetry in Three-Dimensional Flows," *Experiments in Fluids*, Vol. 15, No. 2, 1993, pp. 133–146.

[24]Longuet-Higgins, H. C., "A Computer Algorithm for Reconstructing a Scene from Two Projections," *Nature*, Vol. 293, No. 10, 1981, pp. 133–135.

[25]Brill, M. H., Barrett, E. B., and Payton, P. M., "Projective Invariants for Curves in Two and Three Dimensions," *Geometric Invariance in Computer Vision*, edited by J. Mundy and A. Zisserman, MIT Press, Cambridge, MA, 1992, Chap. 9.

[26]Springer, C. E., *Geometry and Analysis of Projective Spaces*, W. H. Freeman and Co., San Francisco, 1964, pp. 18, 19.

[27]Horn, B. K., and Schunck, B. G., "Determining Optical Flow," *Artificial Intelligence*, Vol. 17, No. 1–3, 1981, pp. 185–204.

[28]Haussecker, H., and Fleet, D. J., "Computing Optical Flow with Physical Models of Brightness Variation," *IEEE Transaction on Pattern Analysis and Machine Intelligence*, Vol. 23, No. 6, 2001, pp. 661–673.

[29]Goldstein, R. J., and Kuehn, T. H., "Optical Systems for Flow Measurement: Shadowgraph, Schlieren, and Interferometric Techniques," *Fluid Mechanics Measurements*, 2nd ed., edited by R. J. Goldstein, Taylor and Francis, Washington, DC, 1996, Chap. 7.

[30]Wilders, R. P., Amabile, M. J., Lanzillotto, A-M., and Leu, T.-S., "Recovering Estimates of Fluid Flow from Image Sequence Data," *Computer Vision and Image Understanding*, Vol. 80, No. 2, 2000, pp. 246–266.

J. Gore
Associate Editor